



Buckling curves of stainless steel CHS members: Current state and proposed provisions

Daniel Jindra^{*}, Zdeněk Kala, Jiří Kala

Faculty of Civil Engineering, Brno University of Technology, Veveří 331/95, 602 00 Brno, Czech Republic

ARTICLE INFO

Keywords:

Stainless steel
Flexural buckling
Circular hollow section (CHS)
Finite element modelling (FEM)
First order reliability method
Design methods

ABSTRACT

The study objective is to propose the optimal shape of the flexural buckling curves for stainless steel circular hollow cross-section (CHS) members. It has been pointed out by several researchers, that the currently utilized buckling curves do not fulfil the required structural reliability level, and several provisions have already been proposed. Following this research, our proposals are based on a numerical investigation of the ultimate limit state of geometrically imperfect stainless steel CHS columns of three different material grades (Austenitic 1.4307, Ferritic 1.4003 and Duplex 1.4462) using the statistical characteristics of input initial imperfections, material and geometric parameters. The statistical characteristics are considered according to the results of published research. The first-order reliability method (FORM) supported by the advanced finite element method – geometrically and materially nonlinear imperfect analysis (GMNIA) – is used. The values of the ultimate resistance obtained using FORM are compared with the values of the design resistance determined according to the corresponding European standards and are used to determine the optimal shape of flexural buckling curves. Additionally, the influence of linear correlation between the ultimate resistance of CHS stainless steel columns exposed to flexural buckling and input imperfections is discussed. Studies have shown that the maximum effect of initial axial curvature on resistance occurs at higher slenderness compared to carbon steels. The obtained results present provisions to optimize the flexural buckling curves of stainless steel CHS members and could significantly improve the structural efficiency, resulting in material savings, while preserving the required level of structural reliability.

1. Introduction

Circular hollow section (CHS) steel members, also commonly called round tubes, are widely used because of their wide range of applications in civil engineering. Apart from their aesthetics favoured by architects, structural engineers also appreciate their superior torsional resistance and enhanced bi-axial bending resistance due to the uniform material distribution through the cross-section around the polar axis. From a geometrical point of view, the shape of a circle minimizes the surface area exposed to environmental influences, hence the maintenance requirements are reduced. The application of stainless steel CHS are numerous, ranging from the utilization of tubes as hollow members to various composites, e.g., enhancement of the load-bearing capacity upon filling with concrete [1], carbon fibre-reinforced polymer (CFRP) concrete [2], or even double skin concrete-filled CHS members [3], often utilized in offshore structures [4].

Stainless steel as a material was originally introduced as “rustless

steel” in 1912–1913 [5]. Several grades of stainless steel exist. The most commonly used are duplex, austenitic and ferritic (other grades include martensitic and precipitation hardening stainless steel). The grades differ in microstructure and chemical composition, most importantly in the nickel and chromium content [5].

The utilization of stainless steel is cost-effective for structures exposed to aggressive environments due to its corrosion resistance [6], e.g., for the load-bearing structures of the composite duplex stainless-steel arch bridge in Cala Galdana on the island of Menorca, Spain (2005) [7], or offshore structures [4].

Recent research into stainless steel CHS members includes the study of the application of 3D printing methods (additive manufacturing) by Zhang et al. [8], the investigation of the buckling resistance of CHS members exposed to fire load, e.g., studies by Mohammed and Afshan [9], Mohammed and Cashell [10], Martins et al. [11], He et al. [12], or the study of residual strengths after fire-exposure by He et al. [13]. The flexural buckling capacity of CHS members after fire exposure was

^{*} Corresponding author.

E-mail address: jindra.d@fce.vutbr.cz (D. Jindra).

smaller than the estimation of the appropriate European standard (EC3) [14] for a significant number of specimens [9–13].

However, the design methods of the EC3 [14] do not appear to be conservative enough, and are even rather unsafe for certain values of member slenderness under standard temperature loading conditions, as has already been discussed by several researchers, e.g., Young and Ellobody [15,16], Rasmussen and Rondal [17], Young and Hartono [18], Ashraf et al. [19], Shu et al. [20] or Theofanous et al. [21]. The flexural buckling performance of hot-rolled seamless austenitic stainless steel CHS columns has been recently investigated by Ning et al. [22], and hot-rolled duplex stainless steel CHS columns also by Ning et al. [23], with the conclusion that the predictions of structural resistance based on EC3 are overestimated for certain column slenderness values. This is mainly due to the absence of appropriate experimental data for stainless steel CHS members at the time of publication of the corresponding EC3 standard [17], where mostly experimental data of rectangular or square hollow section members (RHS, SHS) were considered for the EN flexural buckling curve calibration. However, the overall performance of RHS or SHS differs from the performance of CHS mainly due to increased material strength in hardened RHS or SHS corner areas [24].

The production technology of stainless steel has been improving over the last decades and is in general better and more precise than previous carbon steel technology of production. Therefore, the coefficients utilized in the current EC3 design approach might be influenced, especially for shorter members, where the buckling resistance does not have a major impact on global structural resistance. More precise calibration of the current EC3 [14] design approach of stainless steel members is still required, calibration of the coefficients utilized throughout the design process, e.g., partial safety factors, or (which is also an objective of this study) calibration of limit slenderness values $\bar{\lambda}_0$ and imperfection factor α [14].

Experimental data on stainless steel CHS members in compression have been documented. Predominantly austenitic stainless steel (and stub column tests) grades were investigated, e.g., by Talja [25], Rasmussen and Hancock [26], Rasmussen [27], Burgan et al. [28], Gardner and Nethercot [29], Kuwamura [30], Lam and Gardner [31], Zhao et al. [32,33], Uy et al. [34] or Ning et al. [22] (with a focus on flexural buckling). The duplex stainless steel grades CHS stub column tests were conducted by Paquette and Kyriakides [35] and Bardi and Kyriakides [36], and flexural buckling was investigated by Ning et al. [23]. Ferritic stainless steel material grades were tested by Stangenberg [37]. Ample numerical and experimental studies of CHS columns of several material grades (Austenitic, Ferritic and Duplex) under flexural buckling have been carried out by Buchanan et al. [38]. A wide range of column slenderness was considered, and additional loading eccentricities were subsequently introduced in the continuous study by Buchanan et al. [39].

Various design provisions to determine the CHS flexural buckling capacity have been proposed, e.g., certain alternations of flexural buckling curves were recommended by Young and Ellobody [15], Rasmussen and Rondal [17], Theofanous et al. [21], Ning et al. [22,23] or Buchanan et al. [38]. A unified approach to assess the structural behaviour of CHS columns has been proposed by Ma et al. [40] (for Austenitic and Ferritic stainless steel grades), and a machine-learning algorithm to develop a unified design method suitable for various material grades of CHS members was adopted by Xu et al. [41].

In the study presented here, the flexural buckling resistance of CHS columns is investigated utilizing advanced numerical geometrically and materially nonlinear analyses with imperfections (GMNIA) using the ANSYS software [42]. Members of various slenderness and three different material grades are analysed: Austenitic 1.4307, Ferritic 1.4003 and Duplex 1.4462. The first-order reliability method (FORM) utilizing the European standard EN 1990-1-1 [43] is conducted to determine the flexural buckling design resistances based on numerical

finite element analyses. All the necessary statistical values of material parameters along with mutual correlations are adopted according to the statistical research of stainless steel members by Arrayago et al. [44]. A sub-study on the sufficiency of the number of random realizations (sample size) for the FORM is conducted and documented as well. For this sub-study, 4 additional Austenitic material grades were considered. In total, 10 random input parameters are considered (6 material, 3 geometrical and 1 to determine the initial global imperfection), and the statistical distributions are considered as either normal or lognormal, as recommended by Arrayago et al. [44].

The results (ultimate design resistances expressed in a normalized way) obtained from FORM based on advanced numerical analyses are compared with the design resistances in accordance with EN 1993-1-4 [14], for different slenderness values and material grades. Additionally, the results are compared with the flexural buckling curve utilizing design provisions proposed by Buchanan et al. [38] (chosen due to easy potential future implementation into the current EC3 approach [14]). Based on the FORM design resistances and least square method, optimized flexural buckling curves are proposed for the three discussed material grades: Austenitic 1.4307, Ferritic 1.4003 and Duplex 1.4462, which is the main objective of this study. Furthermore, correlations between the ultimate resistance of stainless steel CHS columns in compression and all the input parameters are discussed.

2. Ultimate resistance determination

2.1. Eurocode based design resistance of members in flexural buckling

The European standard EN 1993-1-4 [14] was used to determine the design resistance values of structural members under compressive loads exposed to flexural buckling. The design buckling resistance of a member in compression $N_{b,Rd}$ for cross-section classes 1–3 is determined as:

$$N_{b,Rd} = \frac{\chi \cdot A \cdot \sigma_{0.2,n}}{\gamma_{M1}}, \quad (1)$$

where γ_{M1} ($\gamma_{M1} = 1.1$ is recommended for stainless steel members) is a partial factor for resistance of members to instability assessed by member checks (buckling resistance) [14]. $\sigma_{0.2,n}$ is the 0.2% proof stress (nominal value), A is the cross-section area (nominal value), and the reduction factor for the relevant buckling mode χ is defined as:

$$\chi = \min \left\{ 1.0; \frac{1}{\phi + [\phi^2 - \bar{\lambda}^2]^{0.5}} \right\}, \quad (2)$$

where the parameter ϕ is determined as:

$$\phi = 0.5 [1 + \alpha(\bar{\lambda} - \bar{\lambda}_0) + \bar{\lambda}^2], \quad (3)$$

where $\bar{\lambda}$ is the global slenderness, $\bar{\lambda}_0$ is the limiting slenderness with the value $\bar{\lambda}_0 = 0.4$ [14], and α is an imperfection factor considered as $\alpha = 0.49$ [14].

In this paper, a validation sub-study (to determine the suitability of the statistic group size) of 6 different global slenderness $\bar{\lambda}$ is conducted, analysing the same CHS 80×1.5 cross-section geometry and 6 different material grades. Subsequently, the main analyses of tubular members of 10 different global slenderness $\bar{\lambda}$ exposed to flexural buckling are performed. In accordance with EN 1993-1-4 [14], the classification of the analysed cross-sections fits within classes 1–3 (for the main part of the study), however, in case of the CHS 80×1.5 utilized for the validation sub-study, the classification covers also section class 4 (for Duplex 1.4462 material grade). The global slenderness values $\bar{\lambda}$ are calculated using Eq. (4) [14] for section classes 1–3, and Eq. (5) for section class 4.

$$\bar{\lambda} = \sqrt{\frac{A \cdot \sigma_{0.2,n} \cdot L^2}{\pi^2 \cdot E \cdot I}}, \quad (4)$$

$$\bar{\lambda} = \sqrt{\frac{A_{eff} \cdot \sigma_{0.2,n} \cdot L^2}{\pi^2 \cdot E \cdot I}} \quad (5)$$

where L is the effective structural length of the column (knife-edge included), E is elastic Young's modulus, $\sigma_{0.2,n}$ is the 0.2% proof stress (nominal value), I is the second-moment area, A is the cross-section area and A_{eff} is the effective cross-sectional area determined in accordance with BS 5950-1 [45]:

$$A_{eff} = \left[\left(\frac{90}{D/t} \right) \cdot \left(\frac{235}{\sigma_{0.2}} \cdot \frac{E}{210000} \right) \right]^{0.5} \quad (6)$$

For the evaluation of the structural resistance, the nominal material parameters were considered according to EN [46]. The product form of a hot-rolled plate is considered. The values are summarized in Table 1 (index "n" stands for nominal value, $\sigma_{u,n}$ is the ultimate stress).

The analysed slenderness ratios are summarized in Table 2 and Table 3 for the validation sub-study and the subsequent main study respectively. Note: some values in the Table 3 are in brackets. It means the results of these cases have not been utilized for further processing, as closely described in chapter 5.

2.2. Structural reliability – First order reliability method (FORM)

In the European standard EN 1990 [43], the reliability design conditions are based on the first-order reliability method (FORM). FORM is one of the most important for the evaluation of structural reliability, mainly in combination with numerical analysis methods, e.g., the finite element method (FEM) as discussed by Faber [47] or Zhao and Ono [48]. The concept of FORM is also described in more detail in studies by Kala [49–51] and Jönsson [52]. The concept of FORM allows the assumption of the Gauss probability density function (PDF) for resistance and load. Since the random variables for the description of the resistance and loading are statistically uncorrelated, the resistance can be studied independently of the load. In this paper, FORM is used to analyse the design resistance of columns under axial compression.

The structural reliability is expressed as a function of random resistance R and random load effect E . The safety margin M is defined as:

$$M = R - E \geq 0. \quad (7)$$

The failure probability P_f is expressed as:

$$P_f = P(R < E) = P(R - E < 0) = P(M < 0), \quad (8)$$

where E and R are statistically independent variables; both defined by Gauss PDF with the mean values μ_E , μ_R , and the standard deviations σ_E , σ_R respectively. M (the safety margin) is described by Gauss PDF defined by mean value μ_M and standard deviation σ_M expressed as:

$$\mu_M = \mu_R - \mu_E, \quad (9)$$

$$\sigma_M = \sqrt{\sigma_R^2 + \sigma_E^2}. \quad (10)$$

The probability of $R - E = M < 0$ is expressed by the integration of PDF of random variable M as:

Table 1
Summary of nominal material parameters for the stainless steel in a product form of hot rolled plate based on EN 1993-1-4.

Material grade	$\sigma_{0.2,n}$ [MPa]	$\sigma_{u,n}$ [MPa]	E_n [GPa]
Austenitic 1.4307	200	500	200
Ferritic 1.4003	250	450	220
Austenitic 1.4318	330	630	200
Austenitic 1.4301	210	520	200
Austenitic 1.4311	270	550	200
Duplex 1.4462	460	640	200

Table 2
Summary of analysed slenderness values for sample size study.

Material grade	CHS section	Length (mean value) [mm]	Slenderness $\bar{\lambda}$	Cross-section class (EN)
Austenitic 1.4307	80 × 1.5	1350	0.49	1
Ferritic 1.4003	80 × 1.5	1350	0.52	2
Austenitic 1.4318	80 × 1.5	1350	0.63	3
Austenitic 1.4301	80 × 1.5	1350	0.50	2
Austenitic 1.4311	80 × 1.5	1350	0.57	2
Duplex 1.4462	80 × 1.5	1350	0.71	4

$$P_f = \int_{-\infty}^0 f_M dm = \Phi\left(\frac{0 - \mu_M}{\sigma_M}\right) = \Phi(-\beta), \quad (11)$$

where the ratio μ_M/σ_M is the reliability index β , and $\Phi()$ is the normalized cumulative Gauss distribution. In accordance with the European standard EN 1990 [43], the required value of the reliability index for structural members is $\beta_d = 3.8$ considering the reliability class RC2, which corresponds with the consequence class CC2, and the reference time of 50 years, see Chapter B.3.2(2) of annex B [43] or application [53]. The failure probability is then equal to $P_f = \Phi(-3.8) = 7.2 \cdot 10^{-5}$. In general, the structural reliability can be verified by the reliability index:

$$\beta = \frac{\mu_M}{\sigma_M} \geq \beta_d. \quad (12)$$

The probabilistic design condition $P_f < P_{fd}$ (where P_{fd} is the target value of the failure probability [43]) is obtained by the substitution of Eq. (12) into Eq. (11). Eq. (10) might be transformed by the introduction of FORM sensitivity factors α_E , and α_R :

$$\sigma_M = \frac{\sigma_R^2 + \sigma_E^2}{\sqrt{\sigma_R^2 + \sigma_E^2}} = \frac{\sigma_R}{\sqrt{\sigma_R^2 + \sigma_E^2}} \sigma_R + \frac{\sigma_E}{\sqrt{\sigma_R^2 + \sigma_E^2}} \sigma_E, \quad (13)$$

$$\sigma_M = \alpha_R \sigma_R + \alpha_E \sigma_E. \quad (14)$$

In accordance with the European standard [43], for common design conditions (Gauss PDF, common values of σ_R and σ_E) it is allowed to use constant values $\alpha_R = 0.8$ and $\alpha_E = 0.7$ (Chapter C.7(3) of annex C of EN 1990 [43]). This simplification results in $\sigma_M \approx 0.8 \sigma_R + 0.7 \sigma_E$. The design condition of reliability is obtained by substituting Eq. (9) and Eq. (14) into Eq. (12):

$$\mu_E + \alpha_E \beta_d \sigma_E \leq \mu_R - \alpha_R \beta_d \sigma_R. \quad (15)$$

The design load E_d and the design value of the resistance R_d are expressed by the left and right sides of Eq. (15) respectively. For $\alpha_R = 0.8$, the design resistance is:

$$R_d = \mu_R - 0.8 \beta_d \sigma_R. \quad (16)$$

The probability that the structural resistance is smaller than the design value is expressed as:

$$P(R \leq R_d) = \Phi\left(\frac{\mu_R - \alpha_R \beta_d \sigma_R - \mu_R}{\sigma_R}\right) = \Phi(-\alpha_R \beta_d). \quad (17)$$

In this research, the FORM sensitivity factor for the resistance $\alpha_R = 0.8$ and the value of the reliability index $\beta = \beta_d = 3.8$ are adopted. The probability, that the structural resistance determined by this approach is smaller than the design resistance is $\Phi(-0.8 \cdot 3.8) = 0.118\%$. This value is approximately applicable as a 0.1% quantile of resistance PDF [54–57], hence the values of resistances discussed in this study based on FORM are determined by the use of Eq. (16).

Table 3

Summary of structural lengths L [mm] (mean values) of the analysed columns and slenderness ratios (numbers in brackets represent model cases which are not considered for further processing).

Mat. grade	CHS section (EN class)	Slenderness $\bar{\lambda}$									
		0.15	0.30	0.45	0.60	0.75	0.90	1.05	1.20	1.35	1.65
Austenitic 1.4307	21.3 × 2.3 (1)	–	(202)	303	403	504	605	706	807	908	1109
	48.3 × 4.0 (1)	–	469	703	937	1172	1406	1640	1875	2109	2578
	88.9 × 3.2 (1)	–	904	1356	1807	2259	2711	3163	3615	4067	4970
	139.7 × 4.0 (1)	–	1431	2146	2861	3576	4292	5007	5722	6437	7868
	193.7 × 5.0 (1)	–	1989	2984	3978	4973	5967	6962	7956	8951	10,940
Ferritic 1.4003	21.3 × 2.3 (1)	–	(189)	(284)	378	473	568	662	757	851	1041
	48.3 × 4.0 (1)	–	440	660	879	1099	1319	1539	1759	1979	2418
	88.9 × 3.2 (1)	–	848	1272	1695	2119	2543	2967	3391	3815	4662
	139.7 × 4.0 (1)	–	1342	2013	2684	3355	4026	4697	5368	6039	7381
	193.7 × 5.0 (1)	–	1866	2799	3732	4665	5598	6531	7464	8397	10,263
Duplex 1.4462	21.3 × 2.3 (1)	–	(133)	199	266	332	399	465	532	598	731
	48.3 × 4.0 (1)	(155)	309	464	618	773	927	1082	1236	1391	1700
	88.9 × 3.2 (2)	598	596	894	1192	1490	1788	2086	2383	2681	3277
	139.7 × 4.0 (3)	472	943	1415	1887	2358	2830	3301	3773	4245	5188
	193.7 × 5.0 (3)	656	1312	1967	2623	3279	3935	4590	5246	5902	7214

3. Numerical finite element models (FEM)

ANSYS Classic technology (v.20) [42] with APDL (ANSYS parametric design language) scripts have been utilized to create a parametrized numerical finite element model of tubular members. There were ten input variable parameters: one parameter to describe the amplitude of the initial global geometrical imperfection e_0 , three geometrical parameters, and seven material parameters (as described further in detail).

3.1. Geometry of the model and boundary conditions

The tubular columns of the circular hollow section (CHS) are considered as simply supported (pin-ended). The hinges at both ends of the column allow rotation in one direction ($rot_y \neq 0$, see Fig. 1). The cross-section analysed in the validation sub-study is CHS 80 × 1.5, and the cross-section geometries for the subsequent study are summarized in Table. 3.

A large number of different values of the effective structural length L (additional knife edge lengths l included) are considered to analyse the sufficiently large scale of the slenderness and CHS geometries (for the sub-study $L = 1350$ mm - Table. 2 and for the main study additional 139 unique lengths - Table. 3).

To simulate the pin-ended column boundary condition, the circumferential nodes of the CHS tube end were connected with a single node located on the longitudinal axis of the tube. This is applied at both tube

ends. The distance of this single node from a plane defined by a cross-section of the column end is known as the knife-edge length l and is considered as 15 mm or 75 mm for structural lengths L smaller than 400 mm or larger than 400 mm respectively. The beam connections are modelled utilizing almost ideally stiff elements (in comparison with the tube stiffness). Boundary conditions are introduced through these single nodes. Only rotation along the y -axis of the global coordinate system (GCS) is allowed for these nodes, all other degrees of freedom are constrained. Except of the translation along the z -axis of the GCS (CHS tube axis) of the upper node, which is used for introduction of the loading conducted by a prescribed displacement.

The tubular CHS members are modelled utilizing four-nodal structural shell finite elements (SHELL 181). These elements possess six degrees of freedom (DoF) per node (three translational and three rotational). Reduced integration formulation (one integration point in a planar view, three through the element thickness) has been considered along with the hourglass control feature. The stiffness of these finite elements consists of membrane and bending parts (Mindlin-Reissner theory), with the linear transverse shear deformation effect. To alleviate shear locking, the Bathe-Dvorkin shear strain formulation is utilized [42].

Geometrically, the shell elements used to model the tubular wall of the CHS columns are rectangles, with a maximal edge size of $D/4$ in the longitudinal direction and $D/10$ in the tangential direction (along the circumference) Fig. 1. The parameter D is the outer diameter.

It has been previously validated, that numerical FEM analyses adopting the above-described element formulation (and mesh geometries) resulted in a good agreement with the experimental data [58]. Also, a reasonable balance between the computational time demand and the accuracy of results is obtained.

3.2. Introduction of initial geometrical imperfections

The lowest global buckling modal shapes (the 1st eigenmodes) obtained from the prior modal analyses were utilized to implement the initial global geometrical imperfections e_0 (in the shape of a half-wave sine function). Based on the statistical research by Arrayago et al. [44], the utilized statistical values of mean value $e_{0,mean} = L/3484$ and standard deviation of $e_{0,st.dev} = L/6056$ are independent of the stainless steel grade or type.

The local initial geometrical imperfections were neglected, due to their rather negligible influence on the ultimate resistance value and overall global structural response of the analysed CHS columns [58]. When compared with cold-rolled stainless-steel sections, hot-formed members usually have cross-sections with smaller values of local slenderness and in general, the interactions of local and overall buckling

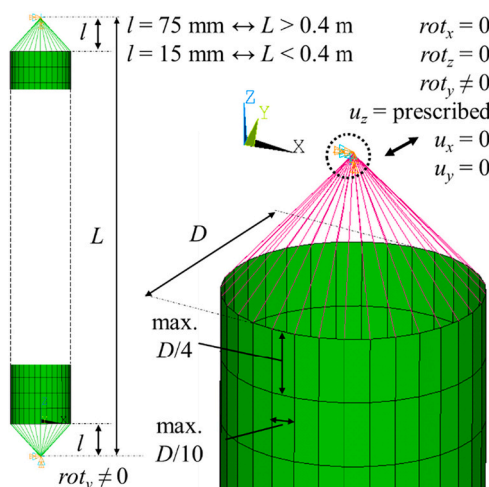


Fig. 1. Numerical FEM model of CHS column; mesh geometry.

modes are not involved in failures [61].

For the initial geometrical imperfection, a lognormal statistical distribution of the input parameter has been considered [44]. Lognormal distribution has been also utilized for concrete-filled steel tubular (CFST) members by Chen et al. [59]. For more complex structures with several components, e.g., truss structure, the imperfection might be implemented as a linear combination of several scaled buckling modes, as performed e.g. by Chen et al. [60]. In this study, only the first buckling mode is utilized, as the geometry is rather simple, hence this approach is sufficient.

3.3. Utilized material model

A suitable stress-strain material relation for stainless steel was proposed by Ramberg and Osgood [61], later modified by Hill [62] and was adopted in this study as the first stage of the material curve:

$$\varepsilon = \frac{\sigma}{E_0} + 0.002 \cdot \left(\frac{\sigma}{\sigma_{0.2}} \right)^n, \quad (18)$$

where σ is the engineering stress and ε is the engineering strain, E_0 is the elastic modulus of the material (Young's modulus), $\sigma_{0.2}$ is the 0.2% proof stress and n is an exponent parameter for strain-hardening description. In the case of using only Eq. (18), the stress values above the 0.2% proof stress $\sigma_{0.2}$ would be overestimated [63]. Hence, a compound two-stage stress-strain relation by Mirambell and Real [64] was introduced, which provides a much better agreement with the experimental data for stress values above the 0.2% proof stress value. A certain modification of the second stage was proposed by Gardner [29] and utilized in this study as well:

$$\varepsilon = \frac{\sigma - \sigma_{0.2}}{E_{0.2}} + \left(\varepsilon_{tu} - \varepsilon_{t0.2} - \frac{\sigma_u - \sigma_{0.2}}{E_{0.2}} \right) \cdot \left(\frac{\sigma - \sigma_{0.2}}{\sigma_u - \sigma_{0.2}} \right)^m + \varepsilon_{t0.2} \Leftrightarrow \sigma > \sigma_{0.2}, \quad (19)$$

where $\varepsilon_{t0.2}$ and ε_{tu} are the total strain at the 0.2% proof stress and the total strain at the ultimate stress σ_u respectively. An exponent parameter m describes the strain hardening above the proof stress value $\sigma_{0.2}$, and $E_{0.2}$ is the stiffness (tangent modulus) at the proof stress $\sigma_{0.2}$ defined as:

$$E_{0.2} = \frac{E_0}{1 + 0.002 \cdot n \cdot \frac{E_0}{\sigma_{0.2}}}, \quad (20)$$

To implement these stress-strain dependencies, a material model with Von Mises plasticity yield surface criterion (isotropic hardening) was adopted. The analytical material curve has been discretized into a multilinear function, considering a sufficient number of small steps. The multilinear material model implementation is described in more detail in the material relation study of the stainless steel [65]. It is also important to note, that the engineering stress-strain material relation (nominal stress and strain) has been transformed into the logarithmic (true) stress-strain notations, as these are required when the geometrically nonlinear analysis is involved [42]:

$$\sigma_{true} = \sigma_{nom} \cdot (1 + \varepsilon_{nom}), \quad (21)$$

$$\varepsilon_{true} = \ln(1 + \varepsilon_{nom}), \quad (22)$$

where the values of stress σ and strain ε (total mechanical strain) are noted with the index "nom" for the engineering notation and with the index "true" for the logarithmic notation. For the compressive material properties, the values of the engineering strain ε_{nom} were introduced with a negative sign. This causes a negative tangent of the stress-strain relation from a certain point, which is in conflict with the standard utilization of the multilinear isotropic hardening material definition [42]. Therefore, a very small positive tangent (ideal plasticity) was considered after the point of the peak logarithmic stress σ_{true} (Fig. 2). The analytical true stress-strain relations are determined considering the

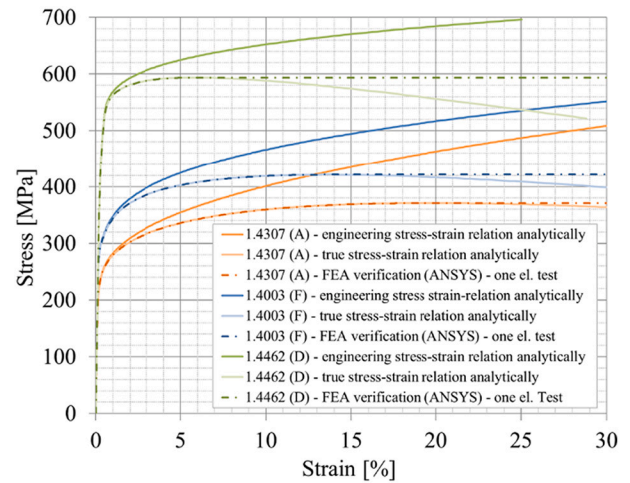


Fig. 2. Material model verifications by one element uniaxial tests.

compressive strain (negative values of ε_{nom} in Eq. (22)). The verification results based on one element test depicted in Fig. 2 are based on a compression of this finite element.

Eq. (19) was used in the second stage of the material model, where the ultimate stress σ_u is utilized to describe the material behaviour, what is well applicable for tensile loading [29]. For compression however, there is no ultimate stress. Hence, more suitable would be to use slightly modified Eq. (23) proposed by Gardner [29], which is in general recommended for combined tension and compression loading as well:

$$\varepsilon = \frac{\sigma - \sigma_{0.2}}{E_{0.2}} + \left(0.008 - \frac{\sigma_{1.0} - \sigma_{0.2}}{E_{0.2}} \right) \cdot \left(\frac{\sigma - \sigma_{0.2}}{\sigma_{1.0} - \sigma_{0.2}} \right)^{m_{0.2,1.0}} + \varepsilon_{t0.2} \Leftrightarrow \sigma > \sigma_{0.2}, \quad (23)$$

where $\sigma_{1.0}$ is the 1% proof stress value, and corresponding exponent parameter $m_{0.2,1.0}$ is used. For the purpose of ultimate resistance determination (with focus on only maximal bearing capacity), it appears to be quite feasible to use both of these Eqs. (19) or (23), with relatively small difference in the results. Comparison of the performance is presented in previous study [66], where stainless I-beam in three point bending test is analysed and material description by both Eqs. (19) and (23) is considered ($\sigma_{1.0}$ value was provided by the inspection certificate). In previous research [76], the Eq. (19) was used, and the final results (buckling curves) were very similar to those presented by Buchanan et al. [38]. It is not assumed there is a significant difference in the results of numerical simulations of CHS members in flexural buckling while using Eqs. (19) or (23), where the main interest is the ultimate resistance value rather than the whole shape of the force-displacement curve.

Advantage of using Eq. (19) in this study is the direct definition of the ultimate stress values σ_u (nominal values) for various material grades in the table 2.1 of EN 1993-1-4 [14], and subsequently the ratios provided by Arrayago et al. [44] to obtain the statistical parameters (mean values and CoV) for σ_u and correlation matrixes between σ_u and the other parameters. On the other hand, 1.0% proof stress is not directly provided in the EN [14], what makes the utilization of Eq. (23) while considering the material values for the corresponding stainless steel grades as defined by the EN [14] less feasible, and would require additional steps in the analysis workflow.

3.4. Residual stresses

During the sectioning process, the released material strips may exhibit curvature and axial deformation, corresponding to bending (through-thickness) and membrane residual stresses, respectively. In general, bending residual stresses dominate in cases of cold-formed sections, and membrane residual stresses are dominant in hot-rolled

sections [67]. The reason for these residual stresses in cases of the hot-rolled steel strips is related to changes in the microstructure during the uneven cooling process [68]. However, in case of the global analysis performed in this study, the residual stresses are incorporated implicitly by the utilization of the measured values of the material properties [69] (more precisely by statistical values based on experimental data) or also considered by the initial geometrical imperfections indirectly [44]. The statistical values (standard deviation and mean value) of all the utilized stainless steel material parameters are based on the study by Arrayago et al. [44], based on data from experimental measurements.

3.5. Validation of the numerical model

The FE model utilized in this study has been previously validated [58], based on experimental data from research conducted by Buchanan et al. [38], where five different cross-sectional geometries of CHS sections have been analysed experimentally and numerically. In total, 37 different stainless steel CHS columns were physically exposed to flexural buckling [38] and force-displacement curves (axial load versus mid-height lateral displacement) were obtained. Two sets of material property values were considered for validation separately. One set is based on the stub column properties (noted as SCP), and the second set is based on tensile properties (TP), as described in more detail by Buchanan et al. [38]. Validation of each set is performed utilizing the arithmetic mean (AM) of the normalized ultimate resistances N_{u} , which is determined as:

$$N_{u, norm, AM} = \frac{1}{37} \sum_{i=1}^{37} \left(\frac{N_{u, FE, i}}{N_{u, exp, i}} \right), \quad (24)$$

where $N_{u, exp}$ stands for the experimentally obtained ultimate resistance and $N_{u, FE}$ is the ultimate resistance based on FEM simulation. The validation average values $N_{u, norm, AM}$ along with its standard deviation bars are graphically depicted for both sets of material properties (SCP, TP) in Fig. 3. All of these normalized values are very close to 1, with small standard deviations, which indicates a very nice match between the numerical simulations and conducted physical experiments [38]. The numerical finite element models utilized in this study can be considered as properly validated [58], hence suitable for the presented reliability analysis.

4. FEM simulations, verifications and reliability analysis

4.1. Input values of statistical parameters

To conduct the first-order reliability analysis (FORM) utilizing GMNIA (geometrically and materially nonlinear imperfect analyses), statistical data on input parameters (material, geometric and imperfection) is required. All of these values are adopted in accordance with the statistical research conducted by Arrayago et al. [44].

Statistical values of all 6 material input parameters (mean values, standard deviation including the utilized distribution type of the probability density function PDF) are summarized in Table 4., which contains the material input data of 3 selected material grades considered for the determination of the buckling curves (the main objective of this

study). Before the main task of this paper was performed, an investigation of the random realization number (sample size study) for the subsequent reliability analysis was conducted. For this, 3 additional material grades of Austenitic steel were considered (1.4301, 1.4311 and 1.4318), and the statistical values are summarized in Table 5. Note: values of parameters E , m , n and ε_u are uniform for all grades of Austenitic stainless steel [44], hence depicted only in the first four rows of Table 4. Statistical values of the geometrical input parameters and the initial global imperfection are summarized in Table 6. These were considered independent of the material grade. Note: the mean values for the structural length L are summarized in Table 2 and Table 3 for the “sample size study” and the “main objective of the paper” respectively. The standard deviation of the structural length L was considered as 0.5 mm, which is half of the smallest unit of standardly used measurement devices.

Correlations between the material input parameters themselves are based on the correlation matrices by Arrayago et al. [44] – see also Fig. 4, Fig. 5 and Fig. 6 for Austenitic, Ferritic and Duplex material grades of stainless steel respectively. Note: the positive correlations are depicted in the shade of blue, the negative ones in red and the larger the correlation, the darker the colour. The correlations between geometrical parameters (D , t , L) are neglected [44], as well as the correlations between initial geometrical imperfection e_0 , and all the other input parameters.

Poisson ratio has been considered with the constant value of $\nu = 0.3$ for all stainless steel grades, analogically to the standard carbon steel material, as discussed in the stochastic sensitivity study by Kala [70].

4.2. FE simulations for the “sample size sub-study”

The sub-study to verify the number of random realization samples per one batch, which is noted as the “sample size sub-study” was conducted before the initiation of the vast number of nonlinear analyses utilized for the subsequent determination of the buckling curves. In this sub-study, 6 material grades (4 Austenitic, one Ferritic and one Duplex) were analysed (summarized in Table 2). One cross-section geometry (CHS 80 × 1.5) along with one structural length of 1350 mm was considered, thus resulting in 6 different slenderness values $\bar{\lambda}$ (dependent on material parameters). For each of the 6 material grades, the ultimate resistance based on FORM was determined three times, each time utilizing one of three unique sample sets of 200 random realizations of all of the 10 input parameters (6 for material, 3 geometrical and one imperfection). These random realizations were generated using the Advanced Latin Hypercube Sampling (ALHS) method, where the correlation errors are minimized by the stochastic evolution strategies [71]. The representation of the specified input correlations and the input distributions is also very accurate when the standard Latin Hypercube Sampling (LHS) method [72] is utilized, where a method by Iman and Conover [73] is implemented to minimize the undesired correlations. ALHS was preferred, as it is recommended for a smaller number of input parameters [74]. To manage the ALHS sampling along with the ANSYS solver, the software OptiSLang [74] was utilized.

In total, 6·3·200 = 3600 numerical simulations were conducted for the sample size study. For each one of these numerical simulations, the ultimate compressive force N_u considered as the maximal value of the force-displacement curve was obtained. A database for the subsequent probabilistic determination of the 0.1% quantile of the N_u was created.

4.3. FE simulations for the buckling curves determinations

After the sample size sub-study had been conducted, it was concluded (see chapters 5.1, 6.1. and 7) that the number of 200 random realizations is sufficient to determine the ultimate resistance based on FORM of a certain model case (unique geometry and material of the CHS column). Hence, in order to obtain a database of results for the sub-

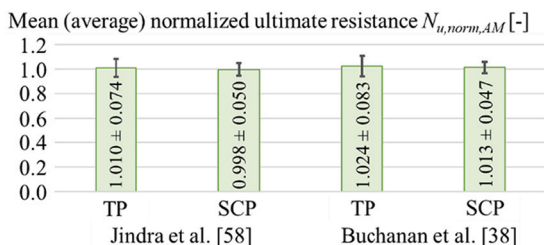


Fig. 3. Numerical finite element model validation.

Table 4
Statistical values of material parameters by Arrayago et al. [44].

Parameter	Unit	Austenitic 1.4307		Ferritic 1.4003		Duplex 1.4462		Distribution type (PDF)
		Mean	St. dev.	Mean	St. dev.	Mean	St. dev.	
Elastic modulus	E [GPa]	195.416	11.175	203.738	14.764	206.233	11.957	Normal
Exponent par.	m [-]	2.3	0.3	2.9	0.3	3.6	0.5	Lognormal
Exponent par.	n [-]	10.6	1.8	16.3	4.9	6.6	2.4	Lognormal
Ultimate strain	ϵ_u [-]	0.49	0.06	0.17	0.05	0.29	0.05	Normal
Ultimate stress	σ_u [MPa]	575	20	504	44.55	704	16.64	Lognormal
0.2% proof stress	$\sigma_{0.2}$ [MPa]	244	15	305	15.75	510.6	44.62	Lognormal

Table 5
Statistical values of material parameters by Arrayago et al. [44].

Parameter	Unit	Austenitic 1.4301		Austenitic 1.4311		Austenitic 1.4318		Distribution type (PDF)
		Mean	St. dev.	Mean	St. dev.	Mean	St. dev.	
Ultimate stress	σ_u [MPa]	598.00	20.80	632.50	22.00	724.50	25.20	Lognormal
0.2% proof stress	$\sigma_{0.2}$ [MPa]	256.20	15.75	329.40	20.25	402.60	24.75	Lognormal

Table 6
Statistical values of geometry and imperfection by Arrayago et al. [44].

Parameter	Unit	Mean value	Standard deviation	Distribution type (PDF)
Diameter	D [mm]	$0.999 \cdot D_n$	$0.003 \cdot D_n$	Normal
Thickness	t [mm]	$0.982 \cdot t_n$	$0.035 \cdot t_n$	Normal
Structural length	L [mm]	various	0.5	Normal
Initial imperfection	e_0 [mm]	$L/3484$	$L/6056$	Lognormal

	E	$\sigma_{0.2}$	n	σ_u	ϵ_u	m
E	1.00	0.143	-0.073	0.277	0.058	-0.107
$\sigma_{0.2}$	0.143	1.00	-0.045	0.855	-0.624	0.263
n	-0.073	-0.045	1.00	-0.277	0.181	-0.283
σ_u	0.277	0.855	-0.277	1.00	-0.534	0.094
ϵ_u	0.058	-0.624	0.181	-0.534	1.00	-0.402
m	-0.107	0.263	-0.283	0.094	-0.402	1.00

Fig. 6. Input correlation matrix for Duplex stainless steels by Arrayago et al. [44].

quent determination of buckling curves, the same approach as described above (Chapter 4.2.) is adopted, with the difference, that only one batch of 200 random realizations of input parameters is performed per model case. For each model case, the unique set of 200 random realizations of 10 input parameters remains. Three different material grades (Austenitic 1.4307, Ferritic 1.4003 and Duplex 1.4462) were investigated. For each material grade, CHS columns of 9 different slenderness λ values of 5 different cross-sectional geometries are analysed. Additional slenderness of 0.15 for 4 different CHS geometries was considered for the Duplex material grade. Therefore, the total number of numerical simulations was equal to 27,800 (3·9·5·200 + 4·200). The summary (according to the mean value of structural length) is also in Table 3. The physical time required for the analysis of one batch of 200 realizations, where realizations were not solved in parallel, ranged from approximately 4 h (for CHS 88.9 × 3.2 of slenderness 0.5) to approximately 7 h (for CHS 88.9 × 3.2 of slenderness 1.65). For each random realization, 4 parallel processes were requested with a single thread per process, with a total of 4 CPU cores requested. A PC with a CPU of 3.6 GHz with 4 cores and 4 threads was utilized.

An example of the correlation matrix of all 10 randomly generated parameters for the model case of Duplex 1.4462 material grade, CHS 88.9 × 3.2, slenderness 1.2 is depicted in the left part of the Fig. 7. The force-displacement curves of all 200 numerical analyses of this model case are depicted in the middle of the Fig. 7. The equivalent plastic strain and horizontal displacement u_x are then provided for a single random realization (order number #125) in the last analysed sub-step (the end of the curve, where $u_x = 23.204$ mm) in the right part of the Fig. 7.

Fig. 4. Input correlation matrix for Austenitic stainless steels by Arrayago et al. [44].

	E	$\sigma_{0.2}$	n	σ_u	ϵ_u	m
E	1.00	-0.122	0.048	-0.124	0.271	-0.16
$\sigma_{0.2}$	-0.122	1.00	-0.341	0.79	-0.757	0.463
n	0.048	-0.341	1.00	-0.341	0.143	-0.30
σ_u	-0.124	0.79	-0.341	1.00	-0.527	0.358
ϵ_u	0.271	-0.757	0.143	-0.527	1.00	-0.457
m	-0.16	0.463	-0.30	0.358	-0.457	1.00

Fig. 5. Input correlation matrix for Ferritic stainless steels by Arrayago et al. [44].

	E	$\sigma_{0.2}$	n	σ_u	ϵ_u	m
E	1.00	-0.063	-0.056	-0.082	0.113	-0.223
$\sigma_{0.2}$	-0.063	1.00	-0.366	0.733	-0.72	0.405
n	-0.056	-0.366	1.00	-0.333	0.49	-0.57
σ_u	-0.082	0.733	-0.333	1.00	-0.503	0.385
ϵ_u	0.113	-0.72	0.49	-0.503	1.00	-0.622
m	-0.223	0.405	-0.57	0.385	-0.622	1.00

Correlation matrix of generated parameters for batch of 200: CHS 88.9×3.2, Duplex 1.4462, $\bar{\lambda} = 1.2$

	D	e ₀	E	L	t	σ _u	ε _u	σ _{0.2}	m	n
D	1.00	0.02	0.00	-0.05	0.04	-0.05	0.03	-0.06	0.01	0.01
e ₀	0.02	1.00	0.02	0.01	0.03	0.00	0.00	0.00	-0.01	-0.02
E	0.00	0.02	1.00	-0.02	0.00	0.28	0.09	0.15	-0.16	-0.05
L	-0.05	0.01	-0.02	1.00	-0.01	0.01	0.00	0.00	0.01	-0.07
t	0.04	0.03	0.00	-0.01	1.00	0.01	0.03	0.00	0.00	-0.06
σ _u	-0.05	0.00	0.28	0.01	0.01	1.00	-0.52	0.87	0.07	-0.25
ε _u	0.03	0.00	0.09	0.00	0.03	-0.52	1.00	-0.61	-0.39	0.16
σ _{0.2}	-0.06	0.00	0.15	0.00	0.00	0.87	-0.61	1.00	0.27	-0.05
m	0.01	-0.01	-0.16	0.01	0.00	0.07	-0.39	0.27	1.00	-0.30
n	0.01	-0.02	-0.05	-0.07	-0.06	-0.25	0.16	-0.05	-0.30	1.00

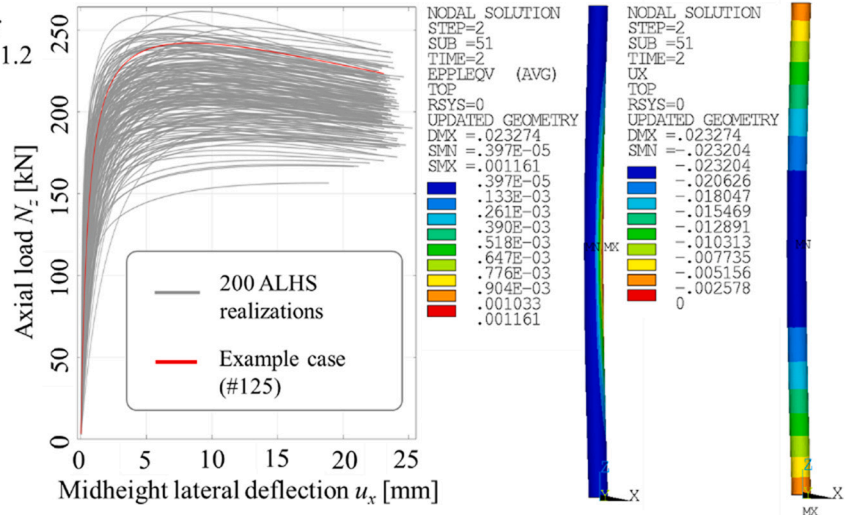


Fig. 7. Example of chosen model case.

4.4. Statistical verification

In order to check the statistical validity of the results, the Gaussian distribution of the results was verified utilizing the Chi-square distribution test or the so-called “goodness-of-fit” test [75]. The purpose of this test is to confirm, that a certain probability distribution (e.g., normal distribution) might be feasibly utilized for the description of a population sample. It was revealed, that the hypothesis of Gauss distribution of the results (ultimate resistance N_u) was not rejected (1% significance level). Therefore, the conclusion of this test is that ultimate resistances N_u based on the finite element simulations might be considered as normally distributed.

4.5. Structural resistance based on first-order reliability method (FORM)

Reliability as described by EC0 [43] is understood as the ability of a structural member (or structure in general) to fulfil certain specified requirements during the whole design lifespan. In case of the ultimate limit state, reliability is considered as the ability to resist the load effects applied on the member.

Following the assumptions of chapter 2.1 of this paper (reliability class RC2, consequence class CC2, 50 years of reference period [43]), the minimal value of the reliability index is $\beta_d = 3.8$, and it is possible to utilize the constant sensitivity factor for the resistance as $\alpha_R = 0.8$. The probability that the resistance is smaller than the design value is then:

$$\Phi(-\alpha_R \beta_d) = \Phi(-0.8 \cdot 3.8) = 0.1183\%. \quad (25)$$

This value approximately corresponds to the 0.1% quantile of the resistance distribution. Therefore, the comparison of the results between the reliability analysis based on FORM and the design resistances calculated according to EC3 [14] is applicable.

For each data set of the 200 random realizations (chapters 4.2. and 4.3.), the standard deviation σ_N , and the mean value μ_N of the ultimate resistance N_u is used to determine the 0.1% resistance quantile $R_{0.1\%}$ considered as the design resistance based on FORM:

$$R_{0.1\%} = \mu_N - \alpha_R \beta_d \sigma_N = \mu_N - 0.8 \cdot 3.8 \cdot \sigma_N. \quad (26)$$

Due to the comparison of several different CHS cross-sectional geometries and various material grades, the ultimate resistance is expressed using the reduction factor χ_{FORM} by substituting $R_{0.1\%}$ for $N_{b,Rd}$ in Eq. (1):

$$\chi_{FORM} = \frac{R_{0.1\%} \cdot \gamma_{M1}}{A \cdot \sigma_{0.2,n}}. \quad (27)$$

The nominal values of proof stress $\sigma_{0.2,n}$ and area A are adopted. The value of the reduction factor χ_{FORM} is determined, which would yield the same design buckling resistance of a member in compression $N_{b,Rd}$ as the resistance based on FORM ($R_{0.1\%}$), utilizing the design approach of the EN [14] and keeping the same value of the partial factor $\gamma_{M1} = 1.1$. This value is compared with the reduction factor χ determined according to the approach of European standard [14] (see chapter 2.1), or with the buckling curve based on EN 1993-1-4 [14].

5. Results

5.1. The sample size sub-study

This sub-study is conducted to investigate the sufficiency of the number of random realizations per one batch (model case). For each of the 6 material grades, 3 different batches of 200 random realizations of all 10 input parameters were analysed, and the ultimate resistance $R_{0.1\%}$ was expressed relatively through the reduction factor χ_{FORM} . The average value of these three reduction factors along with the standard deviation σ and coefficient of variation (CoV) are provided in Table 7, and graphically in Fig. 8, where the values of χ based on EN [14] are also provided. Note: in Table 7, the pure value of the standard deviation is provided ($1 \cdot \sigma$), however, in Fig. 8, $3 \cdot \sigma$ was considered in order to plot the standard deviation bars (due to the small values of σ itself).

5.2. Correlations between the ultimate resistance and input parameters

In order to determine the correlation between ultimate resistance N_u and all the 10 random input parameters, Pearson (linear) correlation

Table 7
Reduction factor χ_{FORM} for CHS 80 × 1.5, L = 1350 mm.

Material grade	Slenderness $\bar{\lambda}$	χ_{FORM} mean	χ_{FORM} standard deviation	χ_{FORM} CoV [%]
Austenitic 1.4307	0.49	0.8604	0.0029	0.34
Ferritic 1.4003	0.52	0.9085	0.0018	0.20
Austenitic 1.4318	0.63	0.8467	0.0011	0.14
Austenitic 1.4301	0.50	0.8612	0.0027	0.31
Austenitic 1.4311	0.57	0.8511	0.0036	0.42
Duplex 1.4462	0.71	0.7287	0.0056	0.76

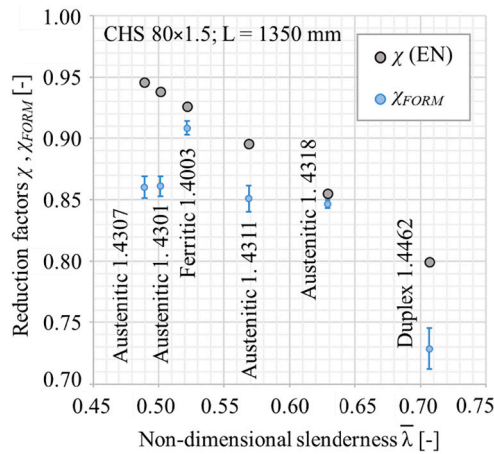


Fig. 8. Determination of reduction factor based on FORM.

coefficient is determined. The values of Pearson correlation coefficient have been averaged for various cross-sectional geometries of the same material grade and slenderness $\bar{\lambda}$ value (average of 5, 4 or 3 values). The arithmetic mean of these correlation coefficients (\pm the standard deviation) are provided in Fig. 9, Fig. 10, and Fig. 11 for Austenitic 1.4307, Ferritic 1.4003 and Duplex 1.4462 material grades respectively. Note: in some cases of smaller slenderness, the average is calculated either from 4 or 3 values. The cases which are represented by numbers in brackets in the Table 3 are excluded for statistic evaluation. For example, in the model case of Duplex 1.4462 material grade and slenderness 0.15, the average is made of 3 different cross-sectional geometries (Table 3). The reason of this is, that some random realizations cases of small slenderness and small structural lengths L resulted in the significantly larger value of ultimate resistances N_u than the average values of that group. As an example, load-deflection curves of the Ferritic grade 1.4003 CHS 21.3×2.3 , slenderness 0.3 are depicted in Fig. 12. Right part of the Fig. 12 depicts the deformed shape along with equivalent plastic strain of FE model of one random realization out of 200 of that case. Different buckling shapes have been mostly observed in cases of smaller values of the initial geometrical imperfections e_0 (smaller structural lengths L) and small slenderness, as discussed also in the previous study [76]. In this study, it has been decided to exclude these cases from further processing.

An example of Anthill plots of random realizations for model cases of Ferritic 1.4003 grade CHS 88.9×3.2 through all the analysed

slenderness values is provided in the left part of the Fig. 13. Right part of the Fig. 13 represents all the other analysed cross-sections for selected slenderness case 1.05 of this material grade. Pearson's correlation coefficients for these selected cases are available in the Fig. 14, and the cells in the matrix corresponds with the cells of the matrix in the Fig. 13. For comparison with linear Pearson's correlations, Kendall τ coefficients of correlation have been determined for these selected cases and are depicted in the matrix in Fig. 15.

Note: For a more transparent graphical depiction (Fig. 9, Fig. 10, Fig. 11, Fig. 14 and Fig. 15), the positive correlations are in shades of blue, negative ones are plotted in red and the darker the colour, the larger the absolute value of the correlation (mean value of the correlation itself for Fig. 9–Fig. 11).

5.3. Determination of the proposed buckling curves

The summary of the reduction factors χ_{FORM} is provided for all analysed model cases (slenderness values, CHS geometries and material grades) in Table 8. In several cases of smaller CHS geometries and smaller slenderness $\bar{\lambda}$ (therefore lengths), the value of the reduction factor happened to be significantly different from the remaining values of the same group (more precisely in 5 cases out of the total 139). For example, CHS 21.3×2.3 , slenderness 0.3 and 0.45 for Ferritic 1.4003 material grade. These values are in brackets in Table 8, as these were not considered for the subsequent averaging and buckling curve determination (the reason is closely described in previous chapter 5.2). For example, in case of CHS 21.3×2.3 , slenderness 0.3 for Ferritic 1.4003 material grade, the mean value μ_N was equal to 40.2737 kN, with the standard deviation of $\sigma_N = 5.9160$ kN (CoV = 14.69%). This results in the reduction factor of 0.714. If 18 of the random realization with the significantly larger N_u (see Fig. 12) were excluded from the set, the mean value μ_N would decrease to 38.8476 kN, and standard deviation σ_N to 2.6373 kN (CoV = 6.79%), resulting in the reduction factor of 0.988, what is in a nice match with the rest of the group. However, exclusion of the whole set was preferred rather than manual alternation of the statistical set. The values of χ_{FORM} (Table 8) of the various cross-sectional geometries (of the same material grade and slenderness value) are averaged (mostly averages of 5 values). Arithmetic means along with standard deviations bars (3σ) are then graphically plotted in Fig. 16 (squares with deviation bars noted as “FORM” in the graph legend). Additionally, the EN buckling curve is provided, as well as the buckling curve based on the provisions proposed by Buchanan et al. [38]. In order to determine a unique buckling curve for each of the three material grades, the least square method has been utilized to optimize the

$\bar{\lambda}$	0.30	0.45	0.60	0.75	0.90	1.05	1.20	1.35	1.65	
Austenitic 1.4307; correlation N_u vs.	D	0.02 ± 0.04	0.03 ± 0.04	0.08 ± 0.02	0.09 ± 0.04	0.11 ± 0.01	0.10 ± 0.02	0.14 ± 0.01	0.10 ± 0.03	0.15 ± 0.04
	e_0	-0.08 ± 0.03	-0.20 ± 0.01	-0.23 ± 0.01	-0.29 ± 0.03	-0.44 ± 0.04	-0.51 ± 0.02	-0.51 ± 0.03	-0.48 ± 0.02	-0.40 ± 0.03
	E	-0.10 ± 0.03	-0.07 ± 0.05	-0.03 ± 0.03	-0.01 ± 0.04	0.15 ± 0.02	0.33 ± 0.03	0.55 ± 0.03	0.69 ± 0.02	0.79 ± 0.02
	L	0.02 ± 0.02	-0.01 ± 0.03	0.01 ± 0.03	0.00 ± 0.02	-0.01 ± 0.02	-0.01 ± 0.02	0.00 ± 0.02	-0.01 ± 0.02	0.00 ± 0.03
	t	0.47 ± 0.02	0.47 ± 0.07	0.52 ± 0.03	0.52 ± 0.03	0.49 ± 0.01	0.48 ± 0.05	0.48 ± 0.04	0.44 ± 0.05	0.43 ± 0.05
	σ_u	0.69 ± 0.02	0.60 ± 0.15	0.59 ± 0.01	0.49 ± 0.03	0.36 ± 0.03	0.19 ± 0.02	0.07 ± 0.03	-0.01 ± 0.04	-0.08 ± 0.01
	ε_u	-0.67 ± 0.01	-0.61 ± 0.12	-0.59 ± 0.03	-0.53 ± 0.03	-0.40 ± 0.02	-0.23 ± 0.02	-0.03 ± 0.01	0.08 ± 0.01	0.20 ± 0.03
	$\sigma_{0.2}$	0.88 ± 0.01	0.78 ± 0.15	0.77 ± 0.02	0.66 ± 0.02	0.51 ± 0.03	0.30 ± 0.02	0.14 ± 0.03	0.02 ± 0.03	-0.07 ± 0.02
	m	0.49 ± 0.05	0.36 ± 0.06	0.30 ± 0.03	0.23 ± 0.02	0.13 ± 0.03	0.01 ± 0.02	-0.04 ± 0.03	-0.10 ± 0.01	-0.14 ± 0.04
	n	-0.38 ± 0.03	-0.16 ± 0.06	-0.01 ± 0.04	0.15 ± 0.03	0.29 ± 0.03	0.35 ± 0.05	0.28 ± 0.01	0.21 ± 0.02	0.10 ± 0.01

Fig. 9. Correlation between the ultimate resistance and input parameters for Austenitic 1.4307 material grade.

$\bar{\lambda}$		0.30	0.45	0.60	0.75	0.90	1.05	1.20	1.35	1.65
Ferritic 1.4003; correlation N_u vs.	D	0.06 ± 0.03	0.05 ± 0.02	0.07 ± 0.02	0.07 ± 0.04	0.09 ± 0.02	0.11 ± 0.03	0.12 ± 0.04	0.12 ± 0.04	0.12 ± 0.02
	e_o	-0.13 ± 0.04	-0.17 ± 0.02	-0.24 ± 0.05	-0.36 ± 0.04	-0.45 ± 0.02	-0.52 ± 0.04	-0.42 ± 0.05	-0.34 ± 0.05	-0.33 ± 0.02
	E	-0.04 ± 0.01	-0.03 ± 0.02	-0.02 ± 0.03	0.08 ± 0.02	0.25 ± 0.03	0.56 ± 0.01	0.75 ± 0.03	0.83 ± 0.02	0.87 ± 0.02
	L	0.03 ± 0.04	0.00 ± 0.01	0.00 ± 0.04	0.00 ± 0.01	-0.01 ± 0.02	0.00 ± 0.01	-0.03 ± 0.03	-0.01 ± 0.03	0.01 ± 0.02
	t	0.50 ± 0.02	0.59 ± 0.01	0.57 ± 0.03	0.51 ± 0.03	0.48 ± 0.04	0.42 ± 0.03	0.39 ± 0.03	0.38 ± 0.06	0.35 ± 0.07
	σ_u	0.64 ± 0.02	0.57 ± 0.03	0.44 ± 0.03	0.31 ± 0.03	0.15 ± 0.03	0.01 ± 0.03	-0.05 ± 0.03	-0.07 ± 0.04	-0.06 ± 0.03
	ε_u	-0.66 ± 0.01	-0.48 ± 0.02	-0.31 ± 0.02	-0.16 ± 0.02	-0.01 ± 0.03	0.10 ± 0.01	0.08 ± 0.02	0.12 ± 0.04	0.10 ± 0.03
	$\sigma_{0.2}$	0.84 ± 0.01	0.77 ± 0.02	0.63 ± 0.04	0.46 ± 0.02	0.27 ± 0.04	0.09 ± 0.02	0.01 ± 0.03	-0.05 ± 0.05	-0.05 ± 0.03
	m	0.43 ± 0.04	0.21 ± 0.03	0.02 ± 0.02	-0.12 ± 0.02	-0.24 ± 0.03	-0.31 ± 0.03	-0.25 ± 0.02	-0.23 ± 0.04	-0.21 ± 0.04
	n	-0.44 ± 0.03	-0.09 ± 0.05	0.18 ± 0.04	0.38 ± 0.02	0.43 ± 0.03	0.32 ± 0.04	0.14 ± 0.03	0.06 ± 0.04	-0.04 ± 0.03

Fig. 10. Correlation between the ultimate resistance and input parameters for Ferritic 1.4003 material grade.

$\bar{\lambda}$		0.15	0.30	0.45	0.60	0.75	0.90	1.05	1.20	1.35	1.65
Duplex 1.4462; correlation N_u vs.	D	0.02 ± 0.02	0.03 ± 0.04	0.05 ± 0.03	0.06 ± 0.04	0.05 ± 0.03	0.03 ± 0.03	0.08 ± 0.02	0.05 ± 0.02	0.12 ± 0.03	0.10 ± 0.03
	e_o	-0.02 ± 0.06	-0.15 ± 0.07	-0.15 ± 0.06	-0.13 ± 0.03	-0.17 ± 0.02	-0.21 ± 0.04	-0.27 ± 0.02	-0.26 ± 0.01	-0.28 ± 0.04	-0.29 ± 0.04
	E	0.09 ± 0.01	0.14 ± 0.08	0.17 ± 0.06	0.17 ± 0.06	0.20 ± 0.01	0.23 ± 0.03	0.26 ± 0.01	0.34 ± 0.02	0.43 ± 0.01	0.62 ± 0.01
	L	0.00 ± 0.04	-0.02 ± 0.04	-0.02 ± 0.04	-0.02 ± 0.02	-0.01 ± 0.01	0.00 ± 0.02	0.01 ± 0.02	-0.02 ± 0.04	-0.01 ± 0.04	0.01 ± 0.02
	t	0.44 ± 0.03	0.37 ± 0.05	0.35 ± 0.06	0.34 ± 0.03	0.37 ± 0.04	0.37 ± 0.04	0.32 ± 0.03	0.34 ± 0.05	0.37 ± 0.05	0.39 ± 0.04
	σ_u	0.73 ± 0.03	0.75 ± 0.05	0.75 ± 0.11	0.78 ± 0.03	0.70 ± 0.02	0.52 ± 0.02	0.38 ± 0.02	0.30 ± 0.04	0.24 ± 0.02	0.20 ± 0.02
	ε_u	-0.60 ± 0.04	-0.61 ± 0.06	-0.56 ± 0.09	-0.56 ± 0.03	-0.49 ± 0.03	-0.35 ± 0.03	-0.23 ± 0.05	-0.14 ± 0.03	-0.11 ± 0.02	0.03 ± 0.01
	$\sigma_{0.2}$	0.84 ± 0.03	0.85 ± 0.08	0.81 ± 0.16	0.90 ± 0.01	0.86 ± 0.01	0.72 ± 0.01	0.59 ± 0.03	0.49 ± 0.03	0.40 ± 0.02	0.25 ± 0.02
	m	0.38 ± 0.04	0.37 ± 0.06	0.33 ± 0.08	0.26 ± 0.04	0.12 ± 0.02	-0.01 ± 0.03	-0.06 ± 0.05	-0.14 ± 0.01	-0.13 ± 0.03	-0.18 ± 0.04
	n	-0.15 ± 0.03	-0.22 ± 0.05	-0.28 ± 0.07	-0.05 ± 0.08	0.22 ± 0.02	0.45 ± 0.03	0.61 ± 0.03	0.63 ± 0.02	0.60 ± 0.02	0.42 ± 0.04

Fig. 11. Correlation between the ultimate resistance and input parameters for Duplex 1.4462 material grade.

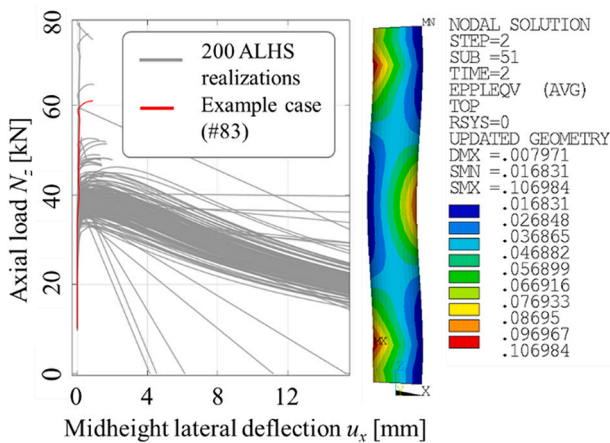


Fig. 12. Example of Ferritic 1.4003 grade, CHS 21.3 × 2.3, slenderness 0.3.

buckling curve parameters $\bar{\lambda}_0$ (limiting slenderness) and α (imperfection factor). Note: for the least square method, values based on Table 8 were used (not the averaged values). The optimal values of $\bar{\lambda}_0$ and α are provided in the legend of Fig. 16.

6. Discussion

6.1. Random realization sample size for FORM analyses

Three different values of reduction factors χ_{FORM} are obtained using three random realizations of $R_{0.1\%}$, where each random realization of $R_{0.1\%}$ is calculated using new 200 samples (random realizations) of input parameters from Tables 4, 5 and 6. This means that each CoV was determined based on a statistic group of three ALHS realizations of 200 samples of random input parameters with the same statistical parameters. The variance of these three random realizations of $R_{0.1\%}$ and χ is relatively small. A variance of zero would theoretically be achieved by increasing from 200 to ∞ samples. For the 200 samples, based on the relatively small values of the coefficients of variation (CoV, Fig. 8 and Table 7), which are below 0.5% for both, Austenitic 1.4307 and Ferritic 1.4003 stainless steels considered in this study, and below 1% for the Duplex 1.4462 stainless steel, the sample size of 200 random realizations is considered to be sufficient enough for the determination of the buckling curves. These values are determined for the slenderness values around 0.5–0.7 (in dependence on the material grade). The largest CoV of 0.76% was obtained for the Duplex stainless steel (slenderness of 0.71). This is also in agreement with the larger standard deviation of χ_{FORM} for the Duplex material grade 1.4462, mainly for the slenderness values of 0.6 and 0.75, when the averaged results are obtained based on

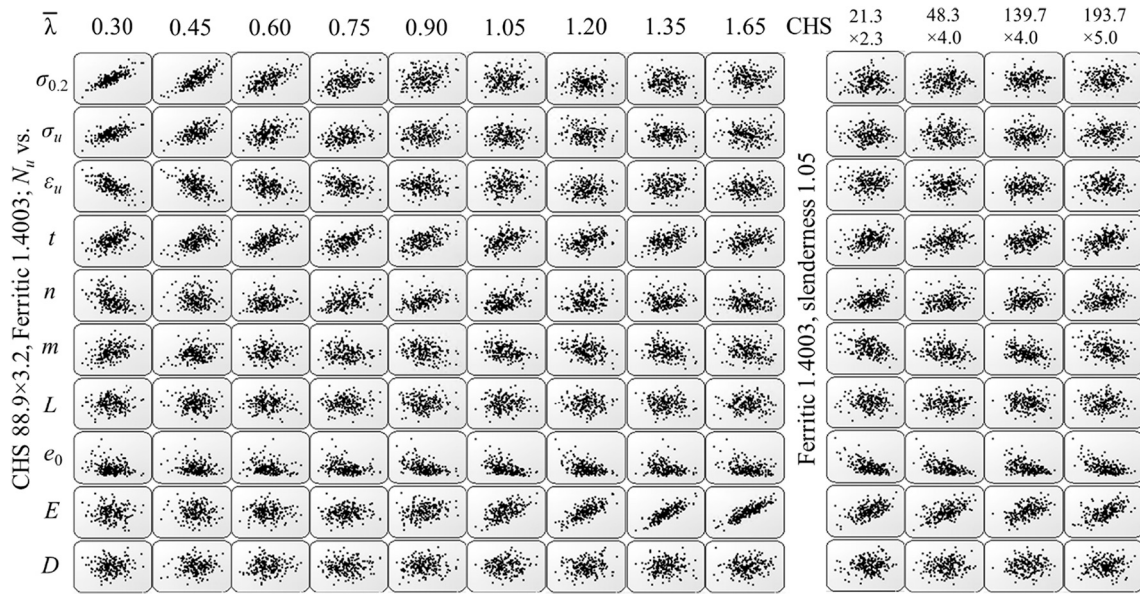


Fig. 13. Example of Anthill plots of random variables for selected cases.

$\bar{\lambda}$	0.30	0.45	0.60	0.75	0.90	1.05	1.20	1.35	1.65	
CHS 88.9x3.2; Ferritic 1.4003; Pearson's correlation coefficients N_u vs.	$\sigma_{0.2}$	0.83	0.77	0.62	0.46	0.26	0.09	0.02	-0.11	-0.05
	σ_u	0.62	0.57	0.44	0.32	0.15	-0.03	-0.08	-0.13	-0.03
	ϵ_u	-0.64	-0.48	-0.31	-0.16	0.01	0.11	0.06	0.14	0.08
	t	0.50	0.60	0.57	0.53	0.53	0.40	0.40	0.44	0.36
	n	-0.41	-0.03	0.18	0.39	0.40	0.37	0.19	0.08	-0.04
	m	0.37	0.20	0.01	-0.13	-0.23	-0.31	-0.27	-0.27	-0.17
	L	0.07	-0.01	-0.02	0.03	0.01	0.01	-0.03	-0.05	0.01
	e_0	-0.16	-0.16	-0.19	-0.32	-0.44	-0.47	-0.46	-0.28	-0.33
	E	-0.05	-0.04	0.00	0.08	0.20	0.56	0.74	0.82	0.86
	D	0.06	0.08	0.08	0.03	0.11	0.12	0.15	0.09	0.11

	CHS	21.3x2.3	48.3x4.0	139.7x4.0	193.7x5.0
Ferritic 1.4003; slenderness 1.05; Pearson's correlation coefficients N_u vs.	$\sigma_{0.2}$	0.11	0.08	0.08	0.11
	σ_u	-0.01	0.04	0.01	0.02
	ϵ_u	0.09	0.12	0.08	0.09
	t	0.38	0.42	0.43	0.46
	n	0.37	0.29	0.30	0.30
	m	-0.35	-0.28	-0.29	-0.30
	L	0.00	0.01	0.01	-0.01
	e_0	-0.57	-0.54	-0.48	-0.54
	E	0.55	0.59	0.55	0.56
	D	0.16	0.08	0.08	0.10

Fig. 14. Pearson's correlation coefficients for the selected model cases.

$\bar{\lambda}$	0.30	0.45	0.60	0.75	0.90	1.05	1.20	1.35	1.65	
CHS 88.9x3.2; Ferritic 1.4003; Kendall τ correlation coefficient N_u vs.	$\sigma_{0.2}$	0.62	0.53	0.42	0.30	0.16	0.04	0.00	-0.04	-0.03
	σ_u	0.42	0.36	0.29	0.20	0.06	-0.02	-0.02	-0.05	-0.04
	ϵ_u	-0.44	-0.31	-0.21	-0.11	-0.01	0.07	0.06	0.09	0.05
	t	0.35	0.40	0.40	0.36	0.33	0.31	0.30	0.27	0.26
	n	-0.29	-0.03	0.12	0.24	0.32	0.23	0.12	0.06	-0.05
	m	0.25	0.07	0.00	-0.09	-0.15	-0.19	-0.17	-0.18	-0.12
	L	0.01	0.02	0.01	0.00	-0.01	0.01	-0.01	-0.02	0.01
	e_0	-0.06	-0.09	-0.15	-0.22	-0.30	-0.33	-0.25	-0.21	-0.18
	E	-0.02	-0.01	0.00	0.06	0.15	0.36	0.53	0.63	0.66
	D	0.03	0.02	0.04	0.01	0.06	0.07	0.08	0.08	0.08

Fig. 15. Kendall τ correlation coefficients for the selected model cases, compared to Fig. 14.

different cross-sectional geometries (Fig. 16). Moreover, the linear correlations between the ultimate resistance and several input parameters with the largest influence for slenderness value 0.6 (e.g., proof stress) are larger (absolutely) for the Duplex material grade (Fig. 11) than Austenitic or Ferritic of the same slenderness value of 0.6 (Fig. 9 and Fig. 10). The standard deviations of the reduction factor χ_{FORM} have been observed smaller for larger values of slenderness, where the results based on different cross-sectional geometries have been averaged (Fig. 16), therefore it is expected that the standard deviations would also be smaller for the ALHS samples of the same statistic values of the input parameters.

6.2. Correlations between the ultimate resistance and input parameters

The results of the linear correlation between the ultimate resistance N_u and input parameters for the Austenitic stainless steel 1.4307 (Fig. 9) are in a good agreement with the previous research [76], where only one cross-sectional geometry of Austenitic stainless steel was analysed (see Fig. 9 in paper [76]). The correlation between the ultimate resistance N_u and the material parameters with a major focus on the description of the plastic behaviour (proof stress, $\sigma_{0.2}$, ultimate stress σ_u , ultimate strain ϵ_u ,

Table 8
Summary of reduction factors χ_{FORM} (numbers in brackets represent cases which are not considered for further processing).

Mat. grade	CHS section (EN class)	Slenderness $\bar{\lambda}$										
		0.15	0.30	0.45	0.60	0.75	0.90	1.05	1.20	1.35	1.65	
Austenitic 1.4307	21.3 × 2.3 (1)	–	(0.870)	0.884	0.832	0.760	0.679	0.597	0.502	0.419	0.291	
	48.3 × 4.0 (1)	–	0.969	0.886	0.823	0.754	0.676	0.595	0.505	0.416	0.289	
	88.9 × 3.2 (1)	–	0.942	0.882	0.816	0.749	0.668	0.588	0.497	0.412	0.284	
	139.7 × 4.0 (1)	–	0.960	0.885	0.813	0.756	0.673	0.585	0.497	0.414	0.281	
	193.7 × 5.0 (1)	–	0.950	0.879	0.813	0.746	0.673	0.583	0.493	0.410	0.281	
Ferritic 1.4003	21.3 × 2.3 (1)	–	(0.714)	(0.890)	0.892	0.816	0.718	0.603	0.486	0.396	0.265	
	48.3 × 4.0 (1)	–	0.989	0.942	0.882	0.804	0.719	0.599	0.484	0.393	0.260	
	88.9 × 3.2 (1)	–	0.992	0.936	0.876	0.801	0.709	0.595	0.483	0.388	0.260	
	139.7 × 4.0 (1)	–	0.980	0.936	0.879	0.800	0.715	0.601	0.487	0.387	0.258	
	193.7 × 5.0 (1)	–	0.981	0.944	0.872	0.799	0.707	0.592	0.489	0.388	0.254	
Duplex 1.4462	21.3 × 2.3 (1)	–	(0.864)	0.841	0.777	0.677	0.584	0.505	0.439	0.380	0.286	
	48.3 × 4.0 (1)	(1.137)	0.907	0.832	0.751	0.663	0.578	0.495	0.429	0.379	0.287	
	88.9 × 3.2 (2)	1.004	0.920	0.830	0.747	0.664	0.577	0.496	0.431	0.373	0.285	
	139.7 × 4.0 (3)	1.019	0.903	0.826	0.732	0.656	0.574	0.494	0.429	0.375	0.281	
	193.7 × 5.0 (3)	1.012	0.914	0.823	0.717	0.655	0.575	0.492	0.426	0.370	0.282	

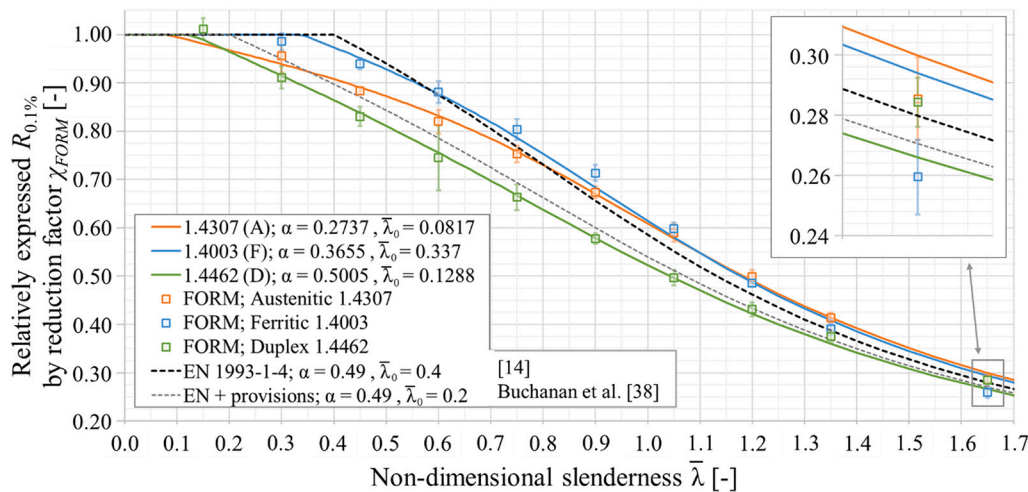


Fig. 16. Buckling curves for stainless steel: current state and proposed provisions.

and exponent parameters n and m) is larger for smaller values of slenderness, where the plastic behaviour of the material is prior to stability loss due to global buckling. Elastic modulus is however more significant for the members of larger slenderness, where the flexural buckling resistance is achieved in a member before reaching the yield stress (proof stress) in its material. From the geometrical parameters, a significant influence on the results is observed for the thickness t , mainly due to its larger input value of the standard deviation (Table 6), which is approximately 12 times larger than the standard deviation of the diameter D , which is easier to sustain during the manufacturing process of the CHS members.

The largest correlation between the resistance N_u and initial geometrical imperfection e_0 is observed around slenderness values $\bar{\lambda} = 1.05\text{--}1.2$ for Austenitic steel (Fig. 9), which is again in agreement with the previous research [76], where the maximum correlation of -0.48 was achieved for the slenderness $\bar{\lambda} = 1.20$.

In general, the correlations between the ultimate resistance N_u and input parameters follow the same pattern in case of the Ferritic (Fig. 10) and Duplex (Fig. 11) stainless steel grades. The differences are in the correlation values themselves, and corresponding slenderness values of correlation extremes for specific parameters. For example, the maximal correlation between the resistance N_u and initial geometrical imperfection e_0 is obtained around slenderness of 1.00 for the Ferritic grade. The Ferritic steels grade 1.4003 is in this matter closer to ordinary carbon steel than the other grades of stainless steel. For carbon steels, the

maximal influence of the geometrical imperfection e_0 on the structural resistance was also observed around the slenderness of 1.0 [70,77]. In the case of Duplex stainless steel, the extreme value of correlation between N_u and e_0 is expected around the slenderness $\bar{\lambda}$ value of 1.65 (Fig. 11). This is an interesting finding that can be important for the design and calibration of buckling curves. However, further analyses would be required to confirm this assumption as the value of 1.65 is also the last analysed slenderness for the Duplex grade in this study.

In this study, it was feasible to utilize linear Pearson's correlation coefficient to determine the correlation between N_u and input parameters. The anthill plots (example in Fig. 13) have not resulted in a shape which would resemble other than linear dependency. The sensitivity ranking of input variables based on the Kendall τ is approximately the same compared to Pearson's correlation (see comparison of Fig. 14 and Fig. 15).

6.3. Buckling curves for CHS stainless steel members

In many of our observations, the design resistances based on FORM analysis have a smaller value than the design resistances according to the current European standard. Therefore, the EC3 design may not be safe enough. In Fig. 16 this might be observed by the data points lying under the EN buckling curve [14] (black curve), mainly for slenderness $\bar{\lambda}$ values around 0.4 for Ferritic 1.4003 stainless steel, and for values between 0.2 and 0.8 for Austenitic 1.4307 stainless steel. This has also

been observed in the previous study [76]. Similar conclusions are made by fellow researchers, e.g. Buchanan et al. [38], and many others [15–23]. For the analysed Duplex stainless steel grade 1.4462, the design approach according to EN [14] is not conservative enough for slenderness $\bar{\lambda}$ values ranging from 0.2 to approximately 1.4. The design provisions of the EN buckling curve proposed by Buchanan et al. [38] have been checked as well (grey buckling curve in Fig. 16). These provisions appear to be rather conservative for Austenitic 1.4307 (which is in agreement with the previous study [76]) and also for Ferritic 1.4003 stainless steel grade. However, in the case of Duplex stainless steel 1.4462, these provisions still are not satisfying enough to fulfil the required structural reliability level (for slenderness values 0.2–1.05). In the case of the Duplex 1.4462 material grade, the performance of the newly proposed buckling curve defined according to the approach of EN [14] with parameters $\bar{\lambda}_0 = 0.1288$ and $\alpha = 0.5005$ appears to be more suitable.

New buckling curves have also been proposed for the Austenitic 1.4307 and Ferritic 1.4003 grades of stainless steel (orange and blue curves in Fig. 16 respectively), with parameters $\bar{\lambda}_0 = 0.0817$ and $\alpha = 0.2737$ for grade 1.4307 (A) and $\bar{\lambda}_0 = 0.337$ and $\alpha = 0.3655$ for 1.4003 (F). These curves appear to utilize the capacity of CHS members in flexural buckling more effectively for slenderness values $\bar{\lambda}$ in the range 0.45–1.2. Therefore, utilization of these new buckling curves might result in significant material savings in comparison with the buckling curve proposed by Buchanan et al. [38], and still retain a sufficient level of structural reliability. On the other hand, for the slenderness $\bar{\lambda}$ above approximately 1.3, the conservativeness of these new curves (A, F, Fig. 16) decreases, and the buckling curve proposed by Buchanan et al. [38] performs much better.

The optimal solution appears to adopt the new proposal for the Duplex stainless steel grade 1.4462 for the whole range of slenderness (curve D, Fig. 16), newly proposed curves, A, F, Fig. 16 for the corresponding material grades for slenderness up to the value of $\bar{\lambda} = 1.2$, linear interpolation between curves A, F, and the buckling curve by Buchanan et al. [38] for slenderness $\bar{\lambda}$ in the range 1.2–1.35, and the curve proposed by Buchanan et al. [38] for the slenderness values over 1.35 (for Austenitic 1.4307 and Ferritic 1.4003 material grades).

Moreover, it appears to be appropriate to check, whether it would be useful to define a unique buckling curve for each grade of stainless steel, e.g., a unique buckling curve for various grades of Austenitic material grades. If the results of Austenitic stainless steel grades analysed in this study presented in Fig. 8 and Fig. 16 are graphically presented together – in Fig. 17, it appears that for the stainless steel grade 1.4318, this might result in a buckling curve of a different shape. It is important to note, that the results for 1.4318 are based only on one cross-sectional

geometry, and also for only one slenderness value. Hence, a more detailed analysis would be required for a proper conclusion. This might be a subject of a future research.

7. Summary

In this study, advanced numerical analyses utilizing the finite element method (FEM) have been used to investigate the flexural buckling resistance of circular hollow section (CHS) stainless steel pin-ended (simply supported) columns of 3 different material grades: Austenitic 1.4307, Ferritic 1.4003 and Duplex 1.4462 (in the hot-rolled product form). In order to describe the nonlinear material behaviour of stainless steel, Eq. (19) which uses ultimate stress has been preferred rather than in general for compressive loading more suitable Eq. (23) which utilizes the 1% proof stress. The reasons are explained in more detail in chapter 3.3.

For each material grade, columns of 9 different slenderness $\bar{\lambda}$ values (within the range 0.2–1.65) have been analysed (with one extra slenderness of 0.15 for the Duplex material). For each of the 9 given slenderness and 3 material grades, numerical analyses of 5 different CHS cross-sectional geometries have been conducted (4 different CHS for the Duplex stainless steel of slenderness 0.15). Altogether, 139 model cases have been numerically analysed. For each model case, a batch of 200 random realizations of 10 statistical input parameters (6 material parameters, 3 geometrical and one initial imperfection) have been calculated. This resulted in a total of 27,800 unique numerical simulations utilizing the ANSYS classic environment. Statistical values of all the input parameters along with their mutual correlations have been utilized according to the comprehensive statistical study by Arrayago et al. [44], where these parameters are summarized based on numerous experimental data.

Moreover, as a prerequisite to this analysis, a shorter sub-study concerning the suitability of the sample size was conducted, where a cross-sectional geometry of CHS 80 × 1.5 was considered for 6 different stainless steel material grades. For each of these 6 cases, the advanced Latin hypercube sampling (ALHS) method was utilized 3 times to create 200 random realizations of the same input of statistical parameters (mean value, standard deviation and mutual correlations). This sub-study of an additional 3600 numerical simulations was conducted to check, whether 200 random realizations is sufficient for each model case, which appeared to be true. Hence the same approach was adopted for the main objective of this research.

For both parts (sub-study and main objective), the advanced geometrically and materially FEM nonlinear analyses with initial imperfections (GMNIA) along with the EC0 approach of the first-order reliability method (FORM) were adopted to determine the design

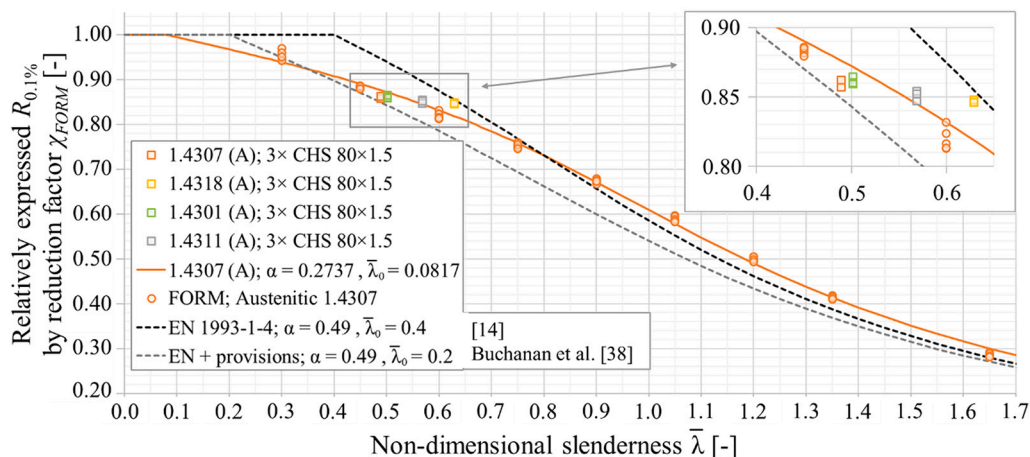


Fig. 17. Buckling curve: various grades of Austenitic stainless steel.

resistances of the columns in flexural buckling. The resistances determined according to this approach are practically the same as the 0.1% quantile of the Gauss distribution of the ultimate resistances N_u .

The main objective of the paper was to determine the ultimate resistance of CHS stainless steel columns exposed to flexural buckling based on the first-order reliability method. These resistances have been expressed relatively by the EN reduction factor χ [14] to be comparable with the Eurocode buckling curve [14] and the buckling curve with design provisions proposed by Buchanan et al. [38] – see Fig. 16. For each of the 3 analysed material grades 1.4307 (A), 1.4003 (F) and 1.4462 (D), a new buckling curve has been determined utilizing the least square method (LSM) and the relatively expressed structural resistances. The definition of these new buckling curves follows the same logic as the current EN [14] approach, where the values of parameters $\bar{\lambda}_0$ (limit slenderness) and α (imperfection factor) have been optimized (by LSM). The proposed values are summarized in the graph legend in Fig. 16.

It also seems, that the results (buckling curves) based on FORM might follow a slightly different pattern for other grades of stainless steel, for example, Austenitic 1.4318 (Fig. 17), which was not investigated in detail in this study, and will be an objective of future research.

8. Conclusion

New buckling curves for stainless steel columns have been proposed using numerical studies and the FORM reliability method. The performance of the new buckling curves is compared and discussed with the current EN buckling curve for stainless steel and with the design provisions by Buchanan et al. [38]. It is concluded, that for Duplex 1.4462 grade, the new proposal appears to be more suitable than the current EN buckling curve. For Ferritic 1.4003 and Austenitic 1.4307 material grades, the new proposals perform better than the current EN buckling curve for slenderness values up to $\bar{\lambda} = 1.2$. However, for values above $\bar{\lambda} = 1.35$, the proposal by Buchanan et al. [38] appears to be the most suitable (compared with the current EN curve and the new proposals presented here). For values in the range 1.2–1.35, linear interpolation between these curves might be easily introduced.

It also appears to be suitable to define a unique flexural buckling curve for several other grades of stainless steel, or at least to check the performance of CHS members of several slenderness values under flexural buckling, e.g., for Austenitic grade 1.4318. This is an objective for future studies.

The conclusions of this study are based on assumption there is very similar output in results while for the second stage of nonlinear material description of stainless steel, either the equation which uses 1% proof stress, or the equation which utilizes the corresponding ultimate stress is used. This assumption appears to be applicable in the scope of the research interest (ultimate resistance value) based on the previous research (chapter 3.3).

CRediT authorship contribution statement

Daniel Jindra: Conceptualization, Methodology, Formal analysis, Writing – original draft, Visualization, Resources, Investigation, Writing – review & editing. **Zdeněk Kala:** Conceptualization, Methodology, Methodology, Supervision, Writing – review & editing, Project administration, Funding acquisition. **Jiří Kala:** Conceptualization, Methodology, Writing – review & editing, Supervision, Data curation.

Declaration of Competing Interest

The authors declare that they have no known competing financial interests or personal relationships that could have appeared to influence the work reported in this paper.

Data availability

Data will be made available on request.

Acknowledgements

This paper was created with the financial support of the Czech Science Foundation by project No.: 20–00761S “Influence of material properties of stainless steels on reliability of bridge structures”. Additional financial support was provided by the Brno University of Technology (BUT) fund for specific university research, the project number FAST-J-22-7816.

References

- [1] Y. Chen, K. Wang, R. Feng, K. He, L. Wang, Flexural behaviour of concrete-filled stainless steel CHS subjected to static loading, *J. Constr. St. Res.* 139 (2017) 30–43, <https://doi.org/10.1016/j.jcsr.2017.09.009>.
- [2] R. Feng, Y. Chen, J. Wei, J. Huang, J. Huang, K. He, Experimental and numerical investigations on flexural behaviour of CFRP reinforced concrete-filled stainless steel CHS tubes, *Eng. Struct.* 156 (2018) 305–321, <https://doi.org/10.1016/j.engstruct.2017.11.032>.
- [3] F. Wang, B. Young, L. Gardner, Compressive testing and numerical modelling of concrete-filled double skin CHS with austenitic stainless steel outer tubes, *Thin-Walled Struct.* 141 (2019) 345–359, <https://doi.org/10.1016/j.tws.2019.04.003>.
- [4] M.F. Hassanein, M. Elchalakani, A. Karrech, V.I. Patel, E. Dacher, Finite element modelling of concrete-filled double-skin short compression members with CHS outer and SHS inner tubes, *Mar. Struct.* 64 (2018) 85–99, <https://doi.org/10.1016/j.marstruc.2018.05.002>.
- [5] L. Gardner, The use of stainless steel in structures, *Prog. Struct. Eng. Mater.* 7 (2) (2005) 45–55, <https://doi.org/10.1002/pse.190>.
- [6] S.M. Daghash, Q. Huang, O.E. Ozbulut, Tensile behavior and cost-efficiency evaluation of ASTM A1010 steel for bridge construction, *J. Bridg. Eng.* 24 (8) (2019) 04019078, [https://doi.org/10.1061/\(ASCE\)BE.1943-5592.0001449](https://doi.org/10.1061/(ASCE)BE.1943-5592.0001449).
- [7] J.A. Sobrino, Stainless steel road bridge in Menorca, Spain, *Struct. Eng. Int.* 16 (2) (2006) 96–100, <https://doi.org/10.2749/10168660677962585>.
- [8] R. Zhang, L. Gardner, C. Buchanan, V.P. Matilainen, H. Piili, A. Salminen, Testing and analysis of additively manufactured stainless steel CHS in compression, *Thin-Walled Struct.* 159 (2021), 107270, <https://doi.org/10.1016/j.tws.2020.107270>.
- [9] A. Mohammed, S. Afshan, Numerical modelling and fire design of stainless steel hollow section columns, *Thin-Walled Struct.* 144 (2019), <https://doi.org/10.1016/j.tws.2019.106243>, 1–13 106243.
- [10] A. Mohammed, K.A. Cashell, Structural behaviour and fire design of duplex and ferritic stainless steel CHS stub columns, *Int. J. Steel Struct.* 21 (2021) 1280–1291, <https://doi.org/10.1007/s13296-021-00502-0>.
- [11] A.D. Martins, R. Goncalves, D. Camotim, Numerical simulation and design of stainless steel columns under fire conditions, *Eng. Struct.* 229 (2021), 111628, <https://doi.org/10.1016/j.engstruct.2020.111628>.
- [12] A. He, Y. Sun, N. Wu, O. Zhao, Testing, simulation and design of eccentrically loaded austenitic stainless steel CHS stub columns after exposure to elevated temperatures, *Thin-Walled Struct.* 164 (2021), 107885, <https://doi.org/10.1016/j.tws.2021.107885>.
- [13] A. He, H.T. Li, X. Lan, Y. Liang, O. Zhao, Flexural buckling behaviour and residual strengths of stainless steel CHS columns after exposure to fire, *Thin-Walled Struct.* 152 (2020), 106715, <https://doi.org/10.1016/j.tws.2020.106715>.
- [14] European Committee for Standardization, Part 1–4: General rules—Supplementary rules for Stainless Steels, in: *EN 1993-1-4:2006+A2: 2020 Eurocode 3—Design of Steel Structures*, Brussels, Belgium, European Committee for Standardization, 2020.
- [15] B. Young, E. Ellobody, Column design of cold-formed stainless steel slender circular hollow sections, *Steel Compos. Struct.* 6 (4) (2006) 285–302, <https://doi.org/10.12989/scs.2006.6.4.285>.
- [16] E. Ellobody, B. Young, Investigation of cold-formed stainless steel non-slender circular hollow section columns, *Steel Compos. Struct.* 7 (4) (2007) 321–337, <https://doi.org/10.12989/scs.2007.7.4.321>.
- [17] K.J.R. Rasmussen, J. Rondal, Column curves for stainless steel alloys, *J. Constr. Steel Res.* 54 (1) (2000) 89–107, [https://doi.org/10.1016/S0143-974X\(99\)00095-4](https://doi.org/10.1016/S0143-974X(99)00095-4).
- [18] B. Young, W. Hartono, Compression tests of stainless steel tubular members, *J. Struct. Eng.* 128 (6) (2002) 754–761, [https://doi.org/10.1061/\(ASCE\)0733-9445\(2002\)128:6\(754\)](https://doi.org/10.1061/(ASCE)0733-9445(2002)128:6(754)).
- [19] M. Ashraf, L. Gardner, D.A. Nethercot, Resistance of stainless steel CHS columns based on cross-section deformation capacity, *J. Constr. Steel Res.* 64 (9) (2008) 962–970, <https://doi.org/10.1016/j.jcsr.2007.10.010>.
- [20] G. Shu, B. Zheng, L. Xin, A new design method for stainless steel columns subjected to flexural buckling, *Thin-Walled Struct.* 83 (2014) 43–51, <https://doi.org/10.1016/j.tws.2014.01.018>.
- [21] M. Theofanous, T.M. Chan, L. Gardner, Structural response of stainless steel oval hollow section compression members, *Eng. Struct.* 31 (4) (2009) 922–934, <https://doi.org/10.1016/j.engstruct.2008.12.002>.

- [22] K. Ning, L. Yang, Y. Sun, Y. Sun, Testing, simulation and design of hot-rolled seamless austenitic stainless steel CHS columns, *Struct.* 40 (2022) 295–302, <https://doi.org/10.1016/j.istruc.2022.04.028>.
- [23] K. Ning, L. Yang, J. Wang, P. Dai, Y. Sun, Experimental and numerical study of hot-rolled duplex stainless steel CHS columns, *J. Constr. Steel Res.* 180 (2021), 106579, <https://doi.org/10.1016/j.jcsr.2021.106579>.
- [24] S. Afshan, B. Rossi, L. Gardner, Strength enhancements in cold-formed structural sections - part I: material testing, *J. Constr. Steel Res.* 83 (2013) 177–188, <https://doi.org/10.1016/j.jcsr.2012.12.008>.
- [25] A. Talja, Test Report on Welded I and CHS Beams, Columns and Beam-Columns, Report to ECSC VTT Building Technology, Technical Research Centre of Finland (VTT), Espoo, Finland, 1997.
- [26] K.J.R. Rasmussen, G.J. Hancock, Design of cold-formed stainless steel tubular members. I: columns, *J. Struct. Eng.* 119 (8) (1993) 2349–2367, [https://doi.org/10.1061/\(ASCE\)0733-9445\(1993\)119:8\(2349\)](https://doi.org/10.1061/(ASCE)0733-9445(1993)119:8(2349)).
- [27] K.J.R. Rasmussen, Recent research on stainless steel tubular structures, *J. Constr. Steel Res.* 54 (1) (2000) 75–88, [https://doi.org/10.1016/S0143-974X\(99\)00052-8](https://doi.org/10.1016/S0143-974X(99)00052-8).
- [28] B.A. Burgan, N.R. Baddoo, K.A. Gilenan, Structural design of stainless steel members - comparison between Eurocode 3, Part 1.4 and test results, *J. Constr. Steel Res.* 54 (1) (2000) 51–73, [https://doi.org/10.1016/S0143-974X\(99\)00055-3](https://doi.org/10.1016/S0143-974X(99)00055-3).
- [29] L. Gardner, D.A. Nethercot, Experiments on stainless steel hollow sections - part 1: material and cross-sectional behaviour, *J. Constr. Steel Res.* 60 (9) (2004) 1291–1318, <https://doi.org/10.1016/j.jcsr.2003.11.006>.
- [30] H. Kuwamura, Local buckling of thin-walled stainless steel members, *Int. J. Steel Struct.* 3 (2003) 191–201.
- [31] D. Lam, L. Gardner, Structural design of stainless steel concrete filled columns, *J. Constr. Steel Res.* 64 (11) (2008) 1275–1282, <https://doi.org/10.1016/j.jcsr.2008.04.012>.
- [32] O. Zhao, L. Gardner, B. Young, Structural performance of stainless steel circular hollow sections under combined axial load and bending - part 1: experiments and numerical modelling, *Thin-Walled Struct.* 101 (2016) 231–239, <https://doi.org/10.1016/j.tws.2015.12.003>.
- [33] O. Zhao, L. Gardner, B. Young, Testing and numerical modelling of austenitic stainless steel CHS beam-columns, *Eng. Struct.* 111 (2016) 263–274, <https://doi.org/10.1016/j.engstruct.2015.12.035>.
- [34] B. Uy, Z. Tao, L.H. Han, Behaviour of short and slender concrete-filled stainless steel tubular columns, *J. Constr. Steel Res.* 67 (3) (2011) 360–378, <https://doi.org/10.1016/j.jcsr.2010.10.004>.
- [35] J.A. Paquette, S. Kyriakides, Plastic buckling of tubes under axial compression and internal pressure, *Int. J. Mech. Sci.* 48 (8) (2006) 855–867, <https://doi.org/10.1016/j.ijmecsci.2006.03.003>.
- [36] F.C. Bardi, S. Kyriakides, Plastic buckling of circular tubes under axial compression - part I: experiments, *Int. J. Mech. Sci.* 48 (8) (2006) 830–841, <https://doi.org/10.1016/j.ijmecsci.2006.03.005>.
- [37] H. Stangenberg, Report to the ECSC - Draft Final Report Ferritic Stainless Steels, Tech. Rep. RWTH, 2000.
- [38] C. Buchanan, E. Real, L. Gardner, Testing, simulation and design of cold-formed stainless steel CHS columns, *Thin-Walled Struct.* 130 (2018) 297–312, <https://doi.org/10.1016/j.tws.2018.05.006>.
- [39] C. Buchanan, O. Zhao, E. Real, L. Gardner, Cold-formed stainless steel CHS beam-columns—testing, simulation and design, *Eng. Struct.* 213 (2020), 110270, <https://doi.org/10.1016/j.engstruct.2020.110270>.
- [40] Y.X. Ma, K.H. Tan, A unified approach for austenitic and ferritic stainless steel CHS beam-columns subjected to eccentric loading, *Thin-Walled Struct.* 165 (2021), 107918, <https://doi.org/10.1016/j.tws.2021.107918>.
- [41] Y. Xu, M. Zhang, B. Zheng, Design of cold-formed stainless steel circular hollow section columns using machine learning methods, *Struct.* 33 (2021) 2755–2770, <https://doi.org/10.1016/j.istruc.2021.06.030>.
- [42] Ansys, Inc, ANSYS 20.0, Ansys, Inc, Canonsburg, PA, USA, 2019.
- [43] European Committee for Standardization, Basis of structural design, in: EN 1990: 2002 Eurocode 0; European Committee for Standardization: Brussels, Belgium, 2002.
- [44] I. Arayago, K.J. Rasmussen, E. Real, Statistical analysis of the material, geometrical and imperfection characteristics of structural stainless steels and members, *J. Constr. Steel Res.* 175 (2020), 106378, <https://doi.org/10.1016/j.jcsr.2020.106378>.
- [45] British Standards Institution, BS 5950-1:2000 structural use of Steelwork in Building - part 1: Code of Practice for Design - Rolled and Welded Sections, 2000.
- [46] European Committee for Standardization, (CEN), EN 10088-4, Stainless Steels Part 4: Technical Delivery Conditions for Sheet/Plate and Strip of Corrosion Resisting Steels for Construction Purposes, Belgium, Brussels, 2009.
- [47] M.H. Faber, Statistics and probability theory, in: Pursuit of Engineering Decision Support, (Part of the Topics in Safety, Risk, Reliability and Quality, book series TSRQ, volume 18) 192, Springer Publishing Company, 2012, https://doi.org/10.1007/978-94-007-4056-3_eISBN:978-94-007-4056-3.
- [48] Y.G. Zhao, T. Ono, A general procedure for first/second-order reliability method (FORM/SORM), *Struct. Saf.* 21 (1999) 95–112.
- [49] Z. Kala, From probabilistic to quantile-oriented sensitivity analysis: new indices of design quantiles, *Symmetry* 12 (10) (2020) 1720, <https://doi.org/10.3390/sym12101720>.
- [50] Z. Kala, Sensitivity analysis in probabilistic structural design: a comparison of selected techniques, *Sustainability* 12 (11) (2020) 4788, <https://doi.org/10.3390/su12114788>.
- [51] Z. Kala, New importance measures based on failure probability in global sensitivity analysis of reliability, *Mathematics* 9 (19) (2021) 2425, <https://doi.org/10.3390/math9192425>.
- [52] J. Jönsson, M.S. Müller, Ch. Gamst, J. Valeš, Z. Kala, Investigation of European flexural and lateral torsional buckling interaction, *J. Constr. Steel Res.* 156 (2019) 105–121, <https://doi.org/10.1016/j.jcsr.2019.01.026>.
- [53] Z. Kala, Reliability analysis of the lateral torsional buckling resistance and the ultimate limit state of steel beams with random imperfections, *J. Civ. Eng. Manag.* 21 (7) (2015) 902–911, <https://doi.org/10.3846/13923730.2014.971130>.
- [54] Z. Kala, J. Valeš, J. Jönsson, Random fields of initial out of straightness leading to column buckling, *J. Civ. Eng. Manag.* 23 (7) (2017) 902–913, <https://doi.org/10.3846/13923730.2017.1341957>.
- [55] Z. Kala, Quantile-based versus Sobol sensitivity analysis in limit state design, *Structures* 28 (2020) 2424–2430, <https://doi.org/10.1016/j.istruc.2020.10.037>.
- [56] Z. Kala, Quantile-oriented global sensitivity analysis of design resistance, *J. Civ. Eng. Manag.* 25 (4) (2019) 297–305, <https://doi.org/10.3846/jcem.2019.9627>.
- [57] Z. Kala, Global sensitivity analysis of quantiles: new importance measure based on superquantiles and subquantiles, *Symmetry* 13 (2) (2021) 263, <https://doi.org/10.3390/sym13020263>.
- [58] D. Jindra, Z. Kala, J. Kala, Validation of stainless-steel CHS columns finite element models, *Materials* 14 (7) (2021) 1785, <https://doi.org/10.3390/ma14071785>.
- [59] S. Chen, C. Hou, H. Zhang, L.H. Han, T.M.M. Reliability-based evaluation for concrete-filled steel tubular (CFST) truss under flexural loading, *J. Constr. Steel Res.* 169 (2020), 106018, <https://doi.org/10.1016/j.jcsr.2020.106018>.
- [60] S. Chen, C. Hou, H. Zhang, L.H. Han, Structural behavior and reliability of CFST trusses with random initial imperfections, *Thin-Walled Struct.* 143 (2019), 106192, <https://doi.org/10.1016/j.tws.2019.106192>.
- [61] W. Ramberg, W.R. Osgood, Description of Stress-Strain Curves by Three Parameters, Technical Note No. 902; National Advisory Committee for Aeronautics: Washington, DC, USA, 1943.
- [62] H.N. Hill, Determination of Stress-Strain Relations from the Offset Yield Strength Values; Technical Note No. 927; National Advisory Committee for Aeronautics: Washington, DC, USA, 1944.
- [63] L. Gardner, D.A. Nethercot, Numerical modelling of cold-formed stainless steel sections, in: Proceedings of the NSCC 2001, 9th Nordic Steel Construction Conference, Helsinki, Finland, 18–20 June 2001, Helsinki University of Technology, Helsinki, Finland, 2001, pp. 781–789.
- [64] E. Mirambell, E. Real, On the calculation of deflections in structural stainless steel beams: an experimental and numerical investigation, *J. Constr. Steel Res.* 54 (1) (2000) 109–133, [https://doi.org/10.1016/S0143-974X\(99\)00051-6](https://doi.org/10.1016/S0143-974X(99)00051-6).
- [65] D. Jindra, Z. Kala, S. Seitl, J. Kala, Material model parameter identification of stainless STEEL (AISI 304L), in: Proceedings of the Engineering Mechanics 2020: Institute of Theoretical and Applied Mechanics of the Czech Academy of Sciences—AS CR: Brno, Czech Republic, 2020, pp. 246–249, <https://doi.org/10.21495/5896-3-246>.
- [66] D. Jindra, Z. Kala, J. Kala, S. Seitl, Experimental and numerical simulation of a three point bending test of a stainless steel beam, *Transp. Res. Proc.* 55 (2021) 1114–1121, <https://doi.org/10.1016/j.trpro.2021.07.183>.
- [67] R.B. Cruise, L. Gardner, Residual stress analysis of structural stainless steel sections, *J. Constr. Steel Res.* 64 (2008) 352–366, <https://doi.org/10.1016/j.jcsr.2007.08.001>.
- [68] S. Witek, A. Milenin, Numerical analysis of temperature and residual stresses in hot-rolled steel strip during cooling in coils, *Arch. Civ. Mech. Eng.* 18 (2) (2018) 659–668, <https://doi.org/10.1016/j.acme.2017.11.002>.
- [69] M. Jandera, L. Gardner, J. Machacek, Residual stresses in cold-rolled stainless steel hollow sections, *J. Constr. Steel Res.* 64 (11) (2008) 1255–1263, <https://doi.org/10.1016/j.jcsr.2008.07.022>.
- [70] Z. Kala, Sensitivity and reliability analysis of lateral-torsional buckling resistance of steel beams, *Arch. Civ. Mech. Eng.* 15 (4) (2015) 1098–1107, <https://doi.org/10.1016/j.acme.2015.03.007>.
- [71] D.E. Hungtington, C.S. Lyrantzis, Improvements to and limitations of Latin hypercube sampling, *Probabilistic. Eng. Mech.* 13 (4) (1998) 245–253, [https://doi.org/10.1016/S0266-8920\(97\)00013-1](https://doi.org/10.1016/S0266-8920(97)00013-1).
- [72] M.D. McKay, R. Beckman, W. Conover, A comparison of three methods for selecting values of input variables in the analysis of output from a computer code, *Technometrics* 21 (2) (1979) 239–245, <https://doi.org/10.1080/00401706.1979.10489755>.
- [73] R.L. Iman, W.J. Conover, A distribution-free approach to inducing rank correlation among input variables, *Commun. Stat. Simul. Comput.* 11 (3) (1982) 311–334, <https://doi.org/10.1080/03610918208812265>.
- [74] Dynardo GmbH, OptiSLang Software Manual: Methods for Multi-Disciplinary Optimization and Robustness Analysis, Weimar. <https://www.ansys.com/products/platform/ansys-optislang>, 2019.
- [75] K. Pearson, X. On the criterion that a given system of deviations from the probable in the case of a correlated system of variables is such that it can be reasonably supposed to have arisen from random sampling, *The London, Edinburgh and Dublin Philosophical Magazine and Journal of Science Series 5* 50 (302) (1900) 157–175, <https://doi.org/10.1080/14786440009463897>.
- [76] D. Jindra, Z. Kala, J. Kala, Flexural buckling of stainless steel CHS columns: reliability analysis utilizing FEM simulations, *J. Constr. Steel Res.* 188 (2022), 107002, <https://doi.org/10.1016/j.jcsr.2021.107002>.
- [77] Z. Kala, J. Valeš, Imperfection sensitivity analysis of steel columns at ultimate limit state, *Arch. Civ. Mech. Eng.* 18 (2018) 1207–1218, <https://doi.org/10.1016/j.acme.2018.01.009>.